Nano Research

ISSN 1998-0124 CN 11-5974/O4
https://doi.org/10.26599/NR.2026.94908782

Research Article

Cu nanoparticles coated with porous N-doped carbon for the selective hydrogenation of quinolines under mild conditions

Guanyu Wang[1,§], Zan Zhang[1,§], Taofen Wang[2], Zuxian Cai[1], Baishu Zheng[1](✉), Zhaoxu Wang[1], Ruirui Yun[3](✉), Zilong Tang[1](✉), Hu Zhou[1](✉)

[1] Key Laboratory of Theoretical Organic Chemistry and Function Molecule of Ministry of Education, Hunan Provincial Key Laboratory of Controllable Preparation and Functional Application of Fine Polymers, Hunan Provincial Key Laboratory of Advanced Materials for New Energy Storage and Conversion, School of Chemistry and Chemical Engineering, Hunan University of Science and Technology, Xiangtan 411201, China

[2] School of Physics and Electronics, Hunan University of Science and Technology, Xiangtan 411201, China

[3] The Key Laboratory of Functional Molecular Solids Ministry of Education, College of Chemistry and Materials Science, Anhui Normal University, Wuhu 214001, China

[§] Guanyu Wang and Zan Zhang contributed equally to this work.

Nano Res., **Just Accepted Manuscript** • https://doi.org/10.26599/NR.2026.94908782

https://www.sciopen.com/journal/1998-0124 on Apr. 28, 2026

TOC Graphic

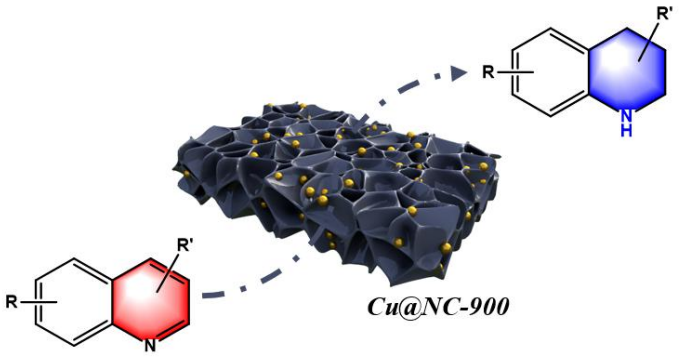

High activity, selectivity and durability

Nano Research

ISSN 1998-0124 CN 11-5974/O4
https://doi.org/10.26599/NR.2026.94908782

Research Article

Cu nanoparticles coated with porous N-doped carbon for the selective hydrogenation of quinolines under mild conditions

Guanyu Wang [1§], Zan Zhang[1§], Taofen Wang[2], Zuxian Cai[1], Baishu Zheng[1](✉), Zhaoxu Wang[1], Ruirui Yun[3] (✉), Zilong Tang[1] (✉), and Hu Zhou[1](✉)

[1] *Key Laboratory of Theoretical Organic Chemistry and Function Molecule of Ministry of Education, Hunan Provincial Key Laboratory of Controllable Preparation and Functional Application of Fine Polymers, Hunan Provincial Key Laboratory of Advanced Materials for New Energy Storage and Conversion, School of Chemistry and Chemical Engineering, Hunan University of Science and Technology, Xiangtan 411201, China*

[2] School of Physics and Electronics, *Hunan University of Science and Technology, Xiangtan 411201, China*

[3] *The Key Laboratory of Functional Molecular Solids Ministry of Education, College of Chemistry and Materials Science, Anhui Normal University, Wuhu 214001, China*

[§] *Guanyu Wang and Zan Zhang contributed equally to this work.*

ABSTRACT

The rational design and construction of high-performance heterogeneous non-noble metal catalysts is an urgent need for the practical application of selective hydrogenation of quinoline and its derivatives. In this work, N-doped porous carbons encapsulated highly-dispersed Cu nanoparticles catalyst (Cu@NC-900) was synthesized by pyrolysis of Cu-MOF precursor, based on the design concept of high efficiency, low cost and excellent durability. Interestingly, the Cu@NC-900 catalyst exhibits extremely high activity, chemo-selectivity and recoverability for the hydrogenation of quinoline and its derivatives using ammonia borane as the hydrogen resources under mild conditions. The characterization results of PXRD, SEM, TEM, Raman spectrum, XPS, EDS and density functional theory (DFT) calculations revealed that the doped N and highly-dispersed Cu species in the catalyst can change the electronic density of the catalyst surface, and thus improve the hydrogenation catalytic performance. This study provides a new idea for rational design of high-performance non-noble metal catalysts for hydrogenation of quinolines under mild conditions.

KEYWORDS

non-noble metal catalysts, density functional theory (DFT), Cu nanoparticles catalyst, hydrogenation of quinoline

1 Introduction

1,2,3,4-tetrahydroquinoline (THQ) and its derivatives are very important N-heterocyclic compounds with a variety of biological activities, and are widely used in pharmaceutical synthesis, gene detection and dyes, etc [1]. At present, the synthesis of THQ mainly includes catalytic cyclization [2], Beckman rearrangement [3] and hydrogenation of quinolines [4]. Among them, selective hydrogenation quinoline to THQ has the advantage of being highly economical, which is in line with the concept of green chemistry and hence considered to be an ideal strategy [5]. However, the reaction of quinoline hydrogenation usually has a high energy barrier, which makes it difficult to be carried out under mild conditions. In addition, the coordination of quinoline and its hydride with the active centre of the catalyst may lead to the poisoning or deactivation of the catalyst, further increasing the difficulty of the reaction. Therefore, the development of efficiently selective catalysts for quinoline hydrogenation is not only challenging, but also of great practical importance.

In recent years, noble metal catalysts (Pd, Pt, Ru, etc) have been widely used in the field of catalytic hydrogenation of quinoline [6-8]. For example, Guo et al. fixed Pd on the amine-rich mesoporous silica hollow nanospheres (HS-NH_2) composite to obtain the ternary composite Pd/HS-NH_2, which has an ultra-high conversion frequency (TOF = 5052 h^{-1}) for quinoline [9]. Dyson et al. reported a Rh NP-Lewis acidic IL catalyst, which has a high selectivity for quinoline hydrogenation at 80~120 ℃ under 30 bar H_2 pressure [10]. Although noble metal heterogeneous catalysis can effectively catalyze such reactions, there are some problems that need to be solved in these systems. For example, the small reserves and high cost of metal materials limit their wide application in practical industrial processes [11]. Therefore, it is urgent to develop efficient and inexpensive heterogeneous catalysts to hydrogenate quinoline. In the past few years, it's worth noting that hydrogenation catalyzed by non-noble metal catalysts (such as Cu [12], Co [13], Ni [14], etc.) has been reported. For example, Li and co-workers optimized the performance of supported Cu monatomic catalyst in selective hydrogenation of quinoline through composite metal oxide strategy [15]. However, the reaction conditions are relatively harsh, usually no less than 80 ℃ and 2.0 MPa H_2 are required to completely convert quinoline to THQ [16-21]. Accordingly, the directional conversion of quinoline to THQ under mild conditions remains one of the major challenges [22]. There is a great need to design multi-purpose non-noble metal catalysts with low cost, high activity and good stability, which is a key step toward replacing noble metal catalysts and is crucial for realizing large-scale industrial production of THQ [23].

In order to achieve high performance conversion of quinoline reduction to THQ, our research group is interested in the design and development of new non-noble metal catalysts using MOF

Address correspondence to Baishu Zheng, zbaishu@163.com; Ruirui Yun, ruirui58@ahnu.edu.cn; Zilong Tang, zltang@hnu.edu.cn; Hu Zhou, zhouhu2006@163.com

materials as the precursor for pyrolysis under the condition of inert gas atmosphere to achieve the goal of low cost, high activity and good stability [24-27]. However, metal nanoparticles supported on MOFs may aggregate or leach the active phase into the reaction solution, resulting in a decreased catalytic activity. One of the most important strategies to enhance the catalytic activity of metal nanoparticles is to modify carbon-based supports via nitrogen (N) doping. The introduction of N dopants creates abundant defective C-N sites and interstitial N species [28-29], which directly modulate the material's catalytic performance by tuning surface reactivity. Beyond this electronic modulation, these structural defects also act as robust anchoring sites, enabling high dispersion of active metal species and maximizing the exposure of accessible catalytic sites [30]. Moreover, N doping profoundly reshapes the spin and charge distribution at the metal-support interface, strengthening the interaction between metal nanoparticles and the N-doped carbon (NC) matrix. This enhanced interaction not only suppresses metal nanoparticle aggregation and leaching but also improves long-term catalytic stability [31-33]. Collectively, the combined effects of defect engineering, electronic modulation, and strong metal-support interaction work synergistically, making NC-supported metal nanoparticles far more active than their counterparts on undoped carbon supports. This phenomenon has been widely validated across different catalytic systems. For instance, Valentina Petrelli *et al.* [34] synthesized two cobalt-based catalysts—Co-pol (N-doped polymer-supported cobalt) and Co-pol2 (a nitrogen-free analog)—to investigate aromatic nitroarene reduction. The results showed that Co-pol2 exhibited drastically lower activity than Co-pol, clearly demonstrating the critical role of nitrogen doping in boosting catalytic performance. In the field of photocatalysis, Xian-He Bu *et al.* [35] prepared NKM-818-BDBPt by introducing amino groups into Zr-MOF ligands. This photocatalyst achieved a hydrogen production rate of 871 μmol g^{-1} h^{-1}, which was 10.62 times higher than that of the nitrogen-free Pt-loaded reference sample (NKM-818@Pt). Notably, the catalytic efficacy of NC supports is closely tied to the bonding configuration of nitrogen dopants, which typically include pyrrolic N, pyridinic N, pyridinic N-oxide, nitrilic N, and graphitic (quaternary) N [36].

In this work, a novel Cu-based nanoparticle catalyst encapsulated in nitrogen-doped porous carbon material (Cu@NC-900) was designed. Cu@NC-900 was prepared by pyrolysis of the Cu-MOF precursor at 900 ℃ under argon flow. Interestingly, very high activity and good selectivity were obtained by competitive reduction of eight quinoline compounds with different functional groups in methanol by Cu@NC-900 at 40 ℃, atmospheric pressure, using ammonborane as the reducing agent. The catalyst has good stability and recyclability, and can be used for 5 cycles without obvious loss of activity. DFT results show that the nitrogen-doped Cu materials can effectively adjust the electronic structure of the catalyst, thereby improve the corresponding catalytic activity.

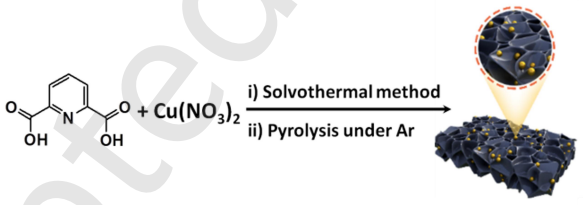

Scheme 1 Illustration of the synthesis of Cu@NC-T catalysts.

2 Results and discussion

Procedures of the preparation of the Cu-based catalyst was shown in Scheme 1. Firstly, the Cu-MOF precursor was prepared by the solvothermal of pyridine-2,6-dicarboxylic acid and $Cu(NO_3)_2 \cdot 3H_2O$. Then, the Cu-MOF material was pyrolyzed in an inert atmosphere to obtain the Cu-based material, which was denoted as Cu@NC-T catalyst (NC = nitrogen-doped porous carbon, T represents the pyrolysis temperature). The structure and phase composition of the Cu-MOF precursor were analyzed by X-ray powder diffraction (PXRD). As shown in Fig. S1, the PXRD pattern of Cu-MOF was in complete agreement with the simulated spectra reported in the literature [37], which confirmed the successful synthesis of the pure phase precursor of Cu-MOF.

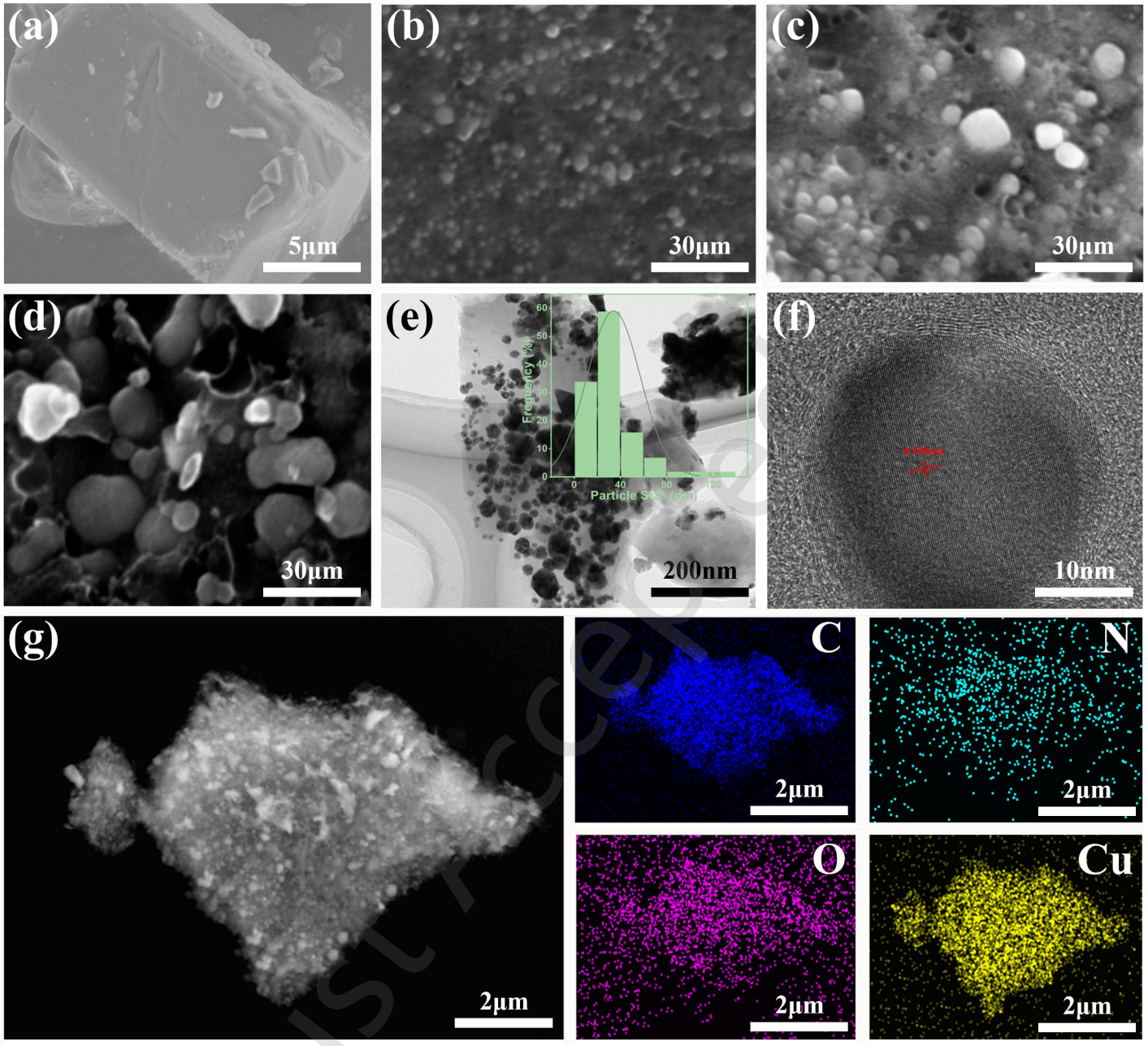

Figure 1 (a-d) SEM images of Cu-MOF, Cu@NC-700, Cu@NC-800 and Cu@NC-900; (e) TEM images and Cu particle size distribution of Cu@NC-900; (f) HAADF-STEM images of Cu@NC-900; (g) EDS-mapping of Cu@NC-900.

The morphology and interior structure properties of the material were characterized using SEM and TEM. Fig. 1 presented the SEM images of Cu-MOF precursors and Cu@NC-T materials, respectively. Obviously, the pyrolysis temperature has an important effect on the morphology and interior structure of the catalytic materials. As the pyrolysis temperature rises, defects start to appear on the surface of the resulting materials. This structural evolution exposes an increasing number of low-coordination Cu atoms, which typically possess higher surface energy and thus serve as highly efficient catalytic active sites. Moreover, HAADF-STEM image and corresponding EDS mapping images of Cu@NC-900 were further used to evaluate the dispersion of Cu NPs in NC support. As shown in Figure 1e-g, the Cu NPs were uniformly distributed on the surfaces of NC matrix, and the C, N and O elements were distributed uniformly. Notably, the average particle size of the Cu NPs on Cu@NC-900 was 34 nm, which was larger than that on Cu@NC-700 (32 nm, see Fig. S2). Moreover, the lattice distances corresponding to the (111) plane of Cu was 0.208 nm, as measured by aberration-corrected high-angle annular dark-field scanning TEM.

Nano Research
ISSN 1998-0124 CN 11-5974/O4
https://doi.org/10.26599/NR.2026.94908782

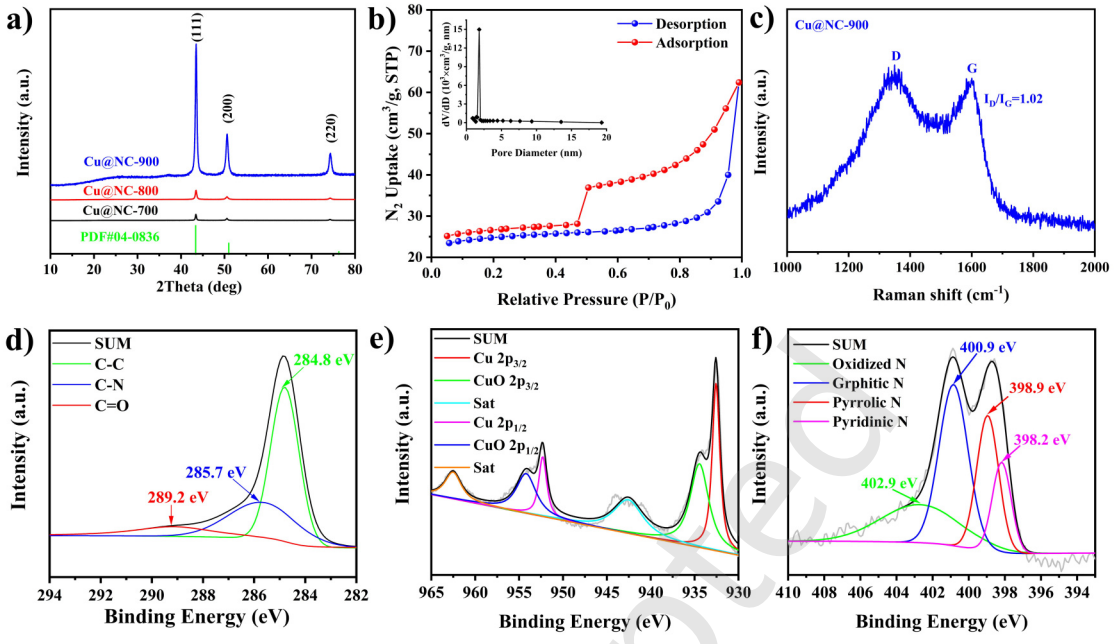

Figure 2 (a) XRD patterns of Cu@NC-700, Cu@NC-800 and Cu@NC-900. (b) Nitrogen adsorption-desorption isotherms of Cu@NC-900 at 77 K, the inset is the pore size distribution. (c) Raman spectrum of Cu@NC-900. (d-f) The C 1s, N 1s and Cu 2p XPS spectra of the Cu@NC-900.

The PXRD patterns of the synthesized Cu@NC-T samples are showed in Fig. 2a, all of the derived samples showed three characteristic peaks in the PXRD patterns at approximately 2θ = 43.3°, 50.4° and 74.1°, corresponding to the (111), (200) and (220) lattice planes of Cu, respectively (PDF card no. 04-0836), which proves the existence of Cu in the catalyst [38]. Additionally, as shown in the Fig. 2a, it can be seen that the diffraction peaks of Cu nanoparticles of Cu@NC-900 were higher in intensity and sharper compared to Cu@NC-700 and Cu@NC-800, indicating that the crystallinity of Cu nanoparticles was increased.

The N_2 adsorption-desorption isotherm of the Cu@NC-900 pyrolyzed sample was characterized to study the specific surface areas and pore structure, which was shown in Fig. 2b. It was apparent that the adsorption and desorption curves of Cu@NC-900 showed a typical type IV isotherm with a H1 type hysteresis loop in the P/P_0 range of 0.4-1.0, indicating the presence of mesoporous structure. This is further confirmed by the pore size distribution in Fig. 2b, Cu@NC-900 sample has a specific surface area of 76.2 $m^2 g^{-1}$ with a pore size of 2 nm. On account of the mesoporous pore size of Cu@NC-900 catalyst, there can be sufficient contact between the active site and the reactant, thus improving the catalytic transfer hydrogenation performance. Furthermore, the structural property of materials was investigated by Raman spectroscopy. As shown in Fig. 2c, the sample showed the clearly visible D-band at 1355 cm^{-1} and G-band at 1590 cm^{-1} for Cu@NC-900, originated from the defective/disordered sp^3 carbon and the in-plane vibrational structure of sp^2 carbon atoms, respectively [39]. On this basis, the formation of graphitic carbon was confirmed. Furthermore, the high I_D/I_G (the intensities ratio of the D and G bands) indicate the presence of strong crystal defects in the N-doped porous carbon material, which can enhance electron transfer and expose enough active sites to potentially accelerate the catalytic reaction.

The XPS characterization of Cu@NC-900 was presented in Fig. 2d-f to reveal the elemental composition and chemical state of the catalysts. The XPS survey spectra indicated that the catalysts contain Cu, C, O and N elements, which were in good agreement with the EDS mapping results. The C1s spectrum of Cu@NC-900 (Fig. 2d) showed that there are three main fitting peaks at the binding energy of 284.8 eV, 285.7 eV and 289.2 eV, corresponding to the peaks of C-C, C=N, and C=O, respectively. The C-C bond is a basic component of the graphite-carbon structure, while the presence of C=N bond indicates that nitrogen atoms have been successfully incorporated into the carbon matrix. This doping not only changes the electronic structure of the carbon matrix, but could also provide additional active sites for catalytic reactions. As far as the Cu 2p XPS spectrum (Fig. 2e) is concerned, the peaks centered at the binding energies of 932.5 eV and 952.3 eV correspond to two peaks of metallic Cu $2p_{3/2}$ and Cu $2p_{1/2}$, respectively [40]. There is an obvious deviation of 19.8 eV between the binding energies, indicating the presence of Cu^0 particles. In the N 1s spectrum, the peaks located at 398.2 eV, 398.9 eV, 400.9 eV and 402.9 eV could be attributed to the corresponded pyridine nitrogen, pyrrole nitrogen, graphite nitrogen and nitrogen oxide, respectively, indicating the successful doping of nitrogen atoms in the carbon matrix (Fig. 2f). These results further confirm the successful doping of Cu and N atoms into the material can provide more catalytic active sites and possibly result in better catalytic effects.

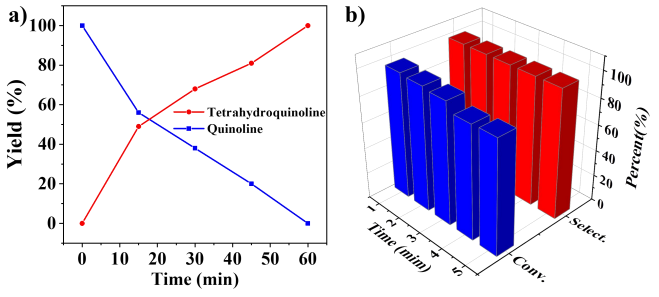

Figure 3 (a) Kinetic curves for hydrogenation of quinoline with Cu/NC-900 as a catalyst. (b) The catalytic performance of the cyclic hydrogenation of quinoline to THQ by Cu@NC-900 catalyst.

The catalytic performance of Cu@NC was studied for the hydrogenation of quinoline to 1,2,3,4-tetrahydroquinoline (THQ) using ammonborane as hydrogen resource and methanol/H_2O as solvent at 40 °C for 1h. The structures of the crude reaction mixtures and target products were determined by ^{1}H-NMR spectra (see Fig. S4−S5). In order to better understand the catalytic activity of Cu@NC, a series of controlled test were conducted, and the results were shown in Table S1. It was observed that the Cu-MOF precursor showed almost no activity for hydrogenation of quinoline, and the catalytic activity significantly increases with increasing pyrolysis temperature for the synthesized Cu@NC-T catalysts. The quinoline conversion of Cu@NC-700 and Cu@NC-800 were only 6.1% and 17.2%, respectively. In contrast, Cu@NC-900 showed superb catalytic activity and achieved extremely high quinoline conversion (~99%) and selectivity (>99%) at 40 °C in a very short time (Fig. 3a). This result indicated that the pyrolysis temperature had a significant effect on the activity of Cu@NC-T catalyst. At 900 °C pyrolysis temperature, combined with the PXRD (Fig. 2a), Raman spectra (Fig. 2c), and XPS data (Fig. 2d-f), it can be seen that Cu@NC-900 formed more metallic Cu nanoparticles and had higher ratio of graphitic nitrogen, further revealing that the synergistic effect of N-doping with graphitic carbon and Cu can lead to high catalytic activity and selectivity. Moreover, compared with other catalysts reported in the literature (Table S2) [15,41-49], the Cu@NC-900 catalyst in this study exhibited higher catalytic performance for the hydrogenation of quinoline under more mild conditions.

In terms of the recyclability and reusability, Cu@NC-900 is easily separated from catalytic reaction systems owning to its inherent magnetic properties, and the recycling experiments show that no significant activity loss occurs during five successive runs (Fig. 3b), indicating the good durability of Cu@NC-900 as a heterogeneous catalyst. In addition, the recovered Cu@NC-900 was also characterized by PXRD (Fig. S6), which confirmed that the Cu@NC-900 catalyst had no obvious difference in crystal structure compared with the fresh-synthesized catalyst, indicating that the Cu@NC-900 catalyst had strong stability under the evaluated reaction conditions.

To demonstrate the general applicability of the prepared Cu@NC-900 catalyst in this study, the selective hydrogenation of various substituted quinolines were further investigated under identical reaction condition, and the results were illustrated in Table. 1. Interestingly, Cu@NC-900 catalyst exhibited exceptional catalytic activity and good selectivity in the hydrogenation of 8 quinoline derivatives. Notably, all the para- and meta-substituted quinoline derivatives with electron-donating (-CH_3, -OH) or electron electronwithdrawing groups (-Cl,-Br,-OCH_3) were fully converted during the reduction, indicating that the steric hindrance does not significantly influence either the catalytic activity and selectivity of the system.

Table 1 Catalytic hydrogenation of different quinoline derivatives with Cu@NC-900.

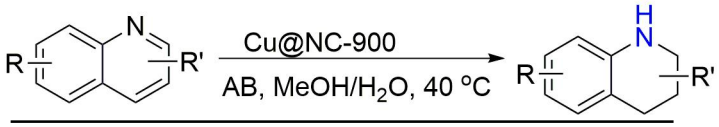

Entry	Product	Time (h)	Con./Sel. (%)[a]
1	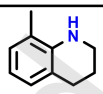	1.5	100/>99
2	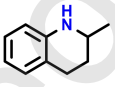	1.5	100/>99
3	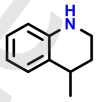	1.5	100/>90
4		1.5	100/>99
5	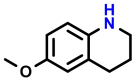	2	100/>99
6		1.5	100/>95
7	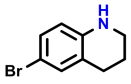	1.5	100/>95
8		1.5	100/>80

[a] Reaction conditions: quinoline derivatives (0.1 mmol), ammonia borane (AB, 1.0 mmol), catalyst (10.0 mg), methanol/H_2O (6.0 mL, 1:2 in volume), 40 ℃.; Conversion and selectivity are determined by gas chromatography-mass spectrometry (GC-MS)(Fig. S3)

Most notably, diverse halogenated substrates with different challenging reducible halogen groups, regardless of their type and location, were successfully and efficiently converted into the corresponding haloaromatic quinolines with no detectable dehalogenation byproducts observed. These results unequivocally demonstrate that in the presence of NH_3·BH_3, the Cu@NC-900 catalyst can efficiently and chemo-selectively catalyze the hydrogenation of quinoline derivatives into the desired tetrahydroquinolines under mild conditions.

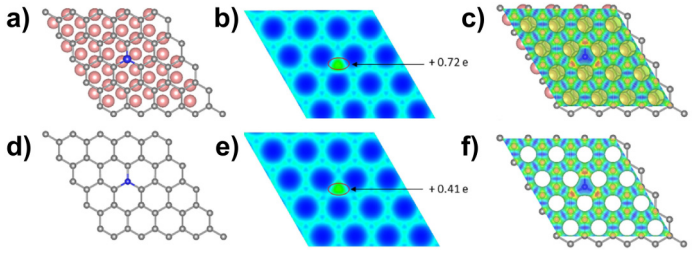

Figure 4 The structure optimization diagrams, charge density 2D distribution diagram and electrostatic potential distribution diagram for Cu@NC (a-c) and NC (d-f).

To explore the synergistic effects of the N-doping and Cu incorporation on the catalytic performance, we performed DFT calculations over the Cu@NC and NC catalysts, respectively. Fig. 4 showed the structure optimization, the 2D charge density distribution and the electrostatic potential distribution maps of Cu@NC and NC, respectively. Compared with NC, the co-doping of Cu and N atoms in Cu@NC materials caused the redistribution of electron density around the Cu center and neighboring N sites, resulting in strong electron aggregation on the surface of Cu@NC. Based on the charge density analysis of Cu@NC and NC, it can be seen that the strong electronegativity mismatch causes electrons to spontaneously transfer from the Cu 3d orbitals to the N 2p orbitals, as evidenced by the increased negative charge of N from -0.41 (in undoped NC) to -0.72 (in Cu@NC). This electronic redistribution facilitates the adsorption of reaction intermediates at the N sites, thereby enhancing catalytic activity. To further elucidate this mechanism, we investigated the adsorption behaviors of quinoline and $NH_3{\cdot}BH_3$ on both catalyst surfaces, with optimized configurations shown in Fig. S7. The calculated adsorption energies for quinoline/aminoborane on Cu@NC (-0.75 eV/-0.36 eV) are significantly lower than those on NC (-0.63 eV/-0.32 eV), indicating stronger substrate binding. The lower adsorption energy on Cu@NC promotes quinoline activation and subsequent hydrogenation,which is consistent with the electronic structure analysis discussed above. These results highlight the critical role of N-Cu co-doping in boosting catalytic performance through synergistic electronic modulation.

The hydrogenation of quinoline to THQ at Cu@NC and NC sites were further investigated. Referring to previous reports on the mechanism of the hydrogenation of quinoline [50-51], The mechanistic investigation of quinoline hydrogenation to 1,2,3,4-tetrahydroquinoline (THQ) on Cu@NC and NC catalysts proceeds via a stepwise pathway: Quinoline → (N-protonation) → int1 (C_9H_8NH) → (C2 hydrogenation) → int2 (1,2-dihydroquinoline) → (C3 hydrogenation) → int3 → (C4 hydrogenation) → THQ*. Fig. 5a showed a possible reaction route of quinoline hydrogenation. The corresponding reaction energy barrier and the corresponding intermediate structure were calculated, as shown in Fig. 5b and Fig. S8. Firstly, the reaction begins with the hydrogenation of the N atom in quinoline and the formation of the intermediate int 1. In this process, the energy barrier on NC was 0.96 eV, while that on Cu@NC was 0.9 eV, indicating that the Cu@NC site was conducive to the hydrogenation of quinoline. Subsequently, the carbon atom next to N is coupled to the hydrogen atom on the catalyst surface to form the partially hydrogenated product 1,2-dihydroquinoline (int 2). The calculated energy barrier decreases from 1.30 eV on NC to 1.26 eV on Cu@NC. The remaining two carbon atoms are hydrogenated to obtain the target product 1,2,3,4-tetrahydroquinoline via the intermediate species int 3. During hydrogenation in H^*-$C_9H_9N^*$, and H^*-$C_9H_{10}N^*$, the energy barrier on Cu@NC was much lower than that on NC (H^*-$C_9H_9N^*$: 0.89 eV vs 0.94 eV; H^*-$C_9H_{10}N^*$: 0.96 eV vs. 5.01 eV). The Cu@NC catalyst, particularly the Cu@NC-900 variant, plays a crucial role by significantly lowering the activation energy barriers for all elementary steps compared to the pure NC site. Most critically, it reduces the prohibitively high energy barrier for the final hydrogenation step (H^*-$C_9H_{10}N^*$, 5.01 eV on NC) to a feasible level (0.96 eV on Cu@NC). This dramatic reduction in the rate-determining step's barrier, attributed to the optimized electronic structure and enhanced adsorption properties induced by the Cu-N-C co-doping effect, is the key factor enabling the efficient and selective hydrogenation of quinoline to THQ on Cu@NC, outperforming the undoped NC catalyst.

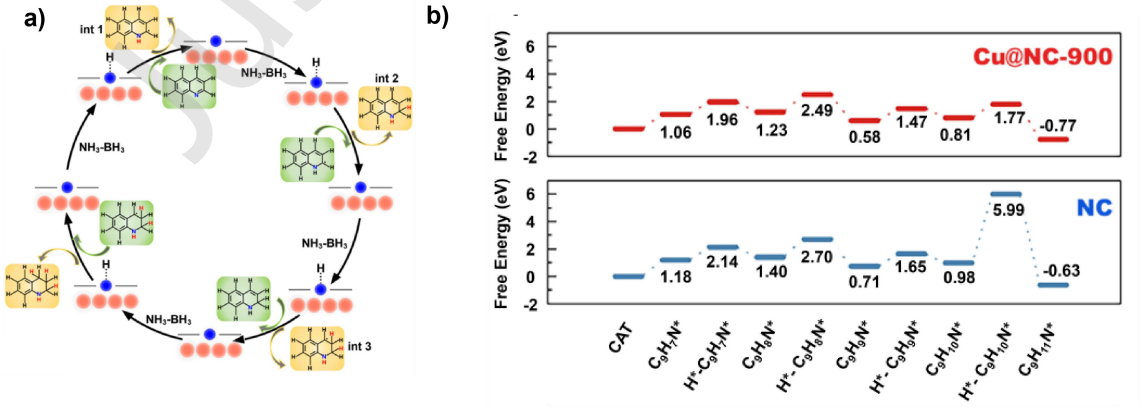

Figure 5 (a) Reaction mechanism of selective hydrogenation of quinolone. (b) Reaction energy barrier diagram.

3 Conclusions

In summary, we have successfully designed and synthesized a nitrogen-doped porous carbon-encapsulated Cu nanoparticle catalyst Cu@NC-900, which exhibited highly catalytic activity and chemical selectivity for the hydrogenation of quinoline and its derivatives under mild reaction conditions. All substrates can be converted to the corresponding THQ with a high conversion rate close to 100% and a selectivity of >90%. The combined characterization results of PXRD, SEM, TEM, Raman spectrum,

XPS and EDS revealed that the high activity and selectivity of Cu@NC-900 can be attributed to the highly dispersed Cu species and doped nitrogen in carbon matrix. Moreover, the Cu@NC-900 catalyst was highly stable and can be reused 5 times without loss of catalytic activity. Furthermore, DFT calculation revealed that there is significant electron redistribution of Cu@NC-900 catalyst in comparison to NC, which greatly improved the catalytic activity of the catalyst. This work may provide a new idea for the rational design of non-noble metal catalysts for hydrogenation of quinolines with high activity, selectivity, and durability.

Acknowledgements

This work was supported by the NSFC (21973029), the Natural Science Foundation of Hunan Province (2024JJ5134,2026JJ80157), the Science and Technology Innovation Program of Hunan Province (2023RC1069), the Scientific Research Fund of Hunan Provincial Education Department (25A0356), and Open Foundation of Hunan Provincial Key Laboratory of Controllable Preparation and Functional Application of Fine Polymers (E22417).

Electronic Supplementary Material: Supplementary material is available in the online version of this article at https://doi.org/10.26599/NR.2026.94908782.

References

[1] Sridharan, V.; Suryavanshi, P. A.; Menéndez, J. C. Advances in the chemistry of tetrahydroquinolines, *Chem. Rev.* **2011**, *111*, 7157–7259.

[2] Omar-Amrani, R.; Thomas, A.; Brenner, E.; Schneider, R.; Fort, Y. Efficient nickel-mediated intramolecular amination of aryl chlorides, *Org. Lett.* **2003**, *5*, 2311–2314.

[3] Maruoka, K.; Miyazaki, T.; Ando, M.; Matsumura,Y.; Sakane,S.; Hattori, K.; Yamamoto, H. Organoaluminum-promoted Beckmann rearrangement of oxime sulfonates, *J. Am. Chem. Soc.* **1983**, *105*, 2831–2843.

[4] Asaula, V. M.; Lytvynenko, A. S.; Mishura, A. M.; Kurmach, M. M.; Buryanov, V. V.; Gavrilenko, K. S.; Ryabukhin, S. V.; Volochnyuk, D. M.; Kolotilov, S. V. In-situ formation of NixB/MIL-101(Cr) and Pd/MIL-101(Cr) composites for catalytic hydrogenation of quinoline, *Inorg. Chem. Commun.* **2020**, *121*, 108203–108206.

[5] Ren, Y. S.; Wang, Y. X.; Li, X.; Zhang, Z. H.; Chi, Q. Selective hydrogenation of quinolines into 1,2,3,4-tetrahydroquinolines over a nitrogen-doped carbon-supported Pd catalyst, *New J. Chem.* **2018**, *42*, 16694–16702.

[6] Li, S. L.; Wang ,L. L.; Wu, M. M.; Sun, Y. F.; Zhu, X. J.; Wan, Y. Measurable surface d charge of Pd as a descriptor for the selective hydrogenation activity of quinolines, *Chin. J. Catal.* **2020**, *41*, 1337–1347.

[7] Zhao, J. B.; Yuan, H. F.; Yang, G.; Liu, Y. F.; Qin, X. M.; Chen, Z.; Weng-Chon, C.; Zhou, L. M.; Fang, S. M. AuPt bimetallic nanoalloys supported on SBA-15: a superior catalyst for quinoline selective hydrogenation in water, *Nano Res.* **2021**, *15*,1796–1802.

[8] Wang, M. D.; Guo, M.; Ren, X. M.; Liu, X.; Yang, Q. H. The influence of surface structure of RhPt bimetallic nanoparticles on the hydrogenation of aromatic compounds, *J. Phys. Chem. C* **2021**, *125*, 15275–15282.

[9] Guo, M.; Li, C.; Yang, Q. H. Accelerated catalytic activity of Pd NPs supported on amine rich silica hollow nanospheres for quinoline hydrogenation, *Catal. Sci. Technol.* **2017**, *7*, 2221–2227.

[10] Karakulina, A.; Gopakumar, A.; Akcok, I.; Roulier, B. L.; LaGrange, T.; Katsyuba, S. A.; Das, S.; Dyson, P. J. A rhodium nanoparticle–Lewis acidic ionic liquid catalyst for the chemoselective reduction of heteroarenes, *Angew. Chem. Int. Ed.* **2016**, *55*, 292–296.

[11] Meemken, F.; Baiker, A. Recent progress in heterogeneous asymmetric hydrogenation of C=O and C=C bonds on supported noble metal catalysts, *Chem. Rev.* **2017**, *117*, 11522–11569.

[12] Shokry, R.; Abd El Salam, H. M.; Aman, D.; Mikhail, S.; Zaki, T.; El Rouby, W. M. A.; Farghali, A. A.; Al Zoubi, W. ; Ko, Y. G. MOF derived core shell MnO@Cu/C as high efficiency catalyst for reduction of nitroarenes, *Chem. Eng. J.* **2023**, *459*, 141554-141563.

[13] Chen, Q. Q.; Jiang, H.; Chen, R. Z. Synthesis of ZIF 67 derived Co-based catalytic membrane for highly efficient reduction of p-nitrophenol, *Chem. Eng. Sci.* **2022**, *248*, 117160-117172.

[14] Wu, J. W.; Liu, W.; Xiang, X.; Sun, K.; Liu, F. H.; Cai, C.; Han, S. B.; Xie, Y. Y. ; Li, S.; Zu, X. T. From $Ni(OH)_2$/graphene composite to Ni@graphene core shell: a self catalyzed epitaxial growth and enhanced activity for nitrophenol reduction, *Carbon* **2017**, 117, 192–200.

[15] Srribes, I.; Liu, L. C.; Dménech-Carbó, A.; Corma, A. Nanolayered cobalt–molybdenum sulfides as highly chemo- and regioselective catalysts for the hydrogenation of quinoline derivatives, *ACS Catal.* **2018**, *8*, 4545–4557.

[16] Dell'Anna, M. M.; Capodiferro, V. F.; Mali ,M.; Manno, D.; Cotugno, P.; Monopoli, A.; Mastrorilli P. Highly selective hydrogenation of quinolines promoted by recyclable polymer supported palladium nanoparticles under mild conditions in aqueous medium, *Appl. Catal. A: Gen.* **2014**, *481*, 89-95.

[17] Ge, D. H.; Hu, L.; Wang, J. Q.; Li, X. M.; Qi, F. Q.; Lu, J. M.; Cao, X. Q.; Gu, H. W. Reversible hydrogenation oxidative dehydrogenation of quinolines over a highly active Pt nanowire catalyst under mild conditions, *ChemCatChem.* **2013**, *5*, 2183-2186.

[18] Xue, X. R.; Zeng, M.; Wang, Y. H. Highly active and recyclable Pt nanocatalyst for hydrogenation of quinolines and isoquinolines, *Appl. Catal. A: Gen.* **2018**, *560*, 37-41.

[19] Zhang, L.; Wang, X. Y.; Xue, Y.; Zeng, X. J.; Chen, H.; Li, R. X.; Wang, S. L. Cooperation between the surface hydroxyl groups of $RuSiO_2$@$mSiO_2$ and water for good catalytic performance for hydrogenation of quinoline, *Catal. Sci. Technol.* **2014**, *4*, 1939-1948.

[20] Zhu, D. M.; Jiang ,H. B.; Zhang, L.; Zheng, X. L.; Fu, H. Y.; Yuan, M. L.; Chen, H.; Li, R. X. Aqueous phase hydrogenation of quinoline to decahydroquinoline catalyzed by ruthenium nanoparticles supported on

glucose derived carbon spheres, *ChemCatChem.* **2014**, *6*, 2954-2960.

[21] Wei, Z. Z.; Chen, Y. Q.; Wang, J.; Su, D. F.; Tang, M. H.; Mao, S. J.; Wang, Y. Cobalt encapsulated in N doped graphene layers: an efficient and stable catalyst for hydrogenation of quinoline compounds, *ACS Catal.* **2016**, *6*, 5816-5822.

[22] Xu, H.; Shi, Z. X.; Tong, Y. X.; Li, G. R. Porous microrod arrays constructed by carbon confined NiCo@$NiCoO_2$ core@shell nanoparticles as efficient electrocatalysts for oxygen evolution, *Adv. Mater.* **2018**, *30*, 1705442-1705449.

[23] She, W.; Qi, T. Q. J.; Cui, M. X.; Yan, P. F.; Ng, S. W.; Li, W. Z.; Li, G. M. High catalytic performance of a CeO_2 -supported Ni catalyst for hydrogenation of nitroarenes, fabricated via coordination assisted strategy, *ACS Appl. Mater. Interfaces.* **2018**, *10*, 14698-14707.

[24] Yun, R. R.; Hong, L. R.; Ma, W. J.; Wang, S. N.; Zheng, B. S. Nitrogen rich porous carbon stabilized Ni Co nanoparticles for the hydrogenation of quinolines, *ACS Appl. Nano Mater.* **2019**, *2*, 6763-6772.

[25] Yun, R. R.; Ma, W. J.; Hong, L. R.; Hu, Y.; Zhan, F. Y.; Liu, S. J.; Zheng, B. S. Ni@PC as a stabilized catalyst toward efficient hydrogenation of quinoline under ambient temperature, *Catal. Sci. Technol.* **2019**, *9*, 6669-6672.

[26] Yun, R .R.; Ma, Z. W.; Hu, Y.; Zhan, F. Y.; Qiu, C.; Zheng, B. S.; Sheng, T. Nano Ni MOFs: high active catalysts for the cascade hydrogenation of quinolines, *Catal. Lett.* **2021**, *151*, 2445-2451.

[27] Yun, R. R.; Zhang, B. B.; Zhan, F. Y.; Du, L. T.; Wang, Z. X.; Zheng, B. S. Cu nanoclusters anchored on the metal organic framework for the hydrolysis of ammonia borane and the reduction of quinolines, *Inorg. Chem.* **2021**, *60*, 12906-12911.

[28] Choi, B.; Yoon, H.; Park, I.-S.; Jang, J.; Sung, Y.-E. Highly Dispersed Pt Nanoparticles on Nitrogen-Doped Magnetic Carbon Nanoparticles and Their Enhanced Activity for Methanol Oxidation, *Carbon* **2007**, *45*, 2496-2501.

[29] Rangraz, Y.; Heravi, M. M.; Elhampour, A. Recent Advances on Heteroatom-Doped Porous Carbon/Metal Materials: Fascinating Heterogeneous Catalysts for Organic Transformations, *Chem. Rec.* **2021**, *21*, 1985-2073.

[30] He, L.; Weniger, F.; Neumann, H.; Beller, M. Synthesis, Characterization, and Application of Metal Nanoparticles Supported on Nitrogen-Doped Carbon: Catalysis beyond Electrochemistry, *Angew. Chem. Int. Ed.* **2016**, *55*, 12582-12594.

[31] Kramer, S.; Mielby, J.; Buss, K.; Kasama, T.; Kegnæs, S. Nitrogen-Doped Carbon-Encapsulated Nickel/Cobalt Nanoparticle Catalysts for Olefin Migration in Allylarenes, *ChemCatChem* **2017**, *9*, 2930-2934.

[32] Gao, D. Z.; Zheng, L. K.; Hu, L. N.; Li, Y.; Liu, H.; Xue, Y. M.; Liu, F.; Zhang, J.; Tang, C. C. Nitrogen-doped carbon nanotubes filled with Fe_3C nanowires for efficient electrocatalytic oxygen reduction, *Colloid Surface A.* **2022**, *654*, 130095-130103.

[33] Zhang, Z.; Liu, Y.; Du, J. F.; Jiang, Y. S.; Wang, Z. X.; Yun, R. R.; Zheng, B. S. Highly efficient hydrogenation of nitroarenes by Co nanoparticles encapsulated in N doped carbon nanotubes under mild conditions, *Inorg. Chem. Front.* **2023**, *10*, 7028–7037.

[34] Petrelli, V.; Romanazzi, G.; Mortalò, C.; Leonelli, C.; Zapparoli, M.; De Giglio, E.; Calvano, C. D.; Dell'Anna, M. M.; Mastrorilli, P. N-Doped Resin Supported Cobalt Nanoparticles for the Catalytic Reduction of Nitroarenes to Corresponding Anilines in Aqueous Medium, *Mol. Catal.* **2023**, *544*, 113050.

[35] Zhang, H.; Shi, Y.; Chen, T.; Fan, Z.; Zhang, T.; Dong, P.; Li, M.; Lang, F.; Yang, K.; Pang, J.; Bu, X.-H. Rational Integration of Amino Functionalization and Catalytic Site Modulation in Zr-MOFs for Synergistic Enhanced Photocatalysis, *Angew. Chem.* **2026**, *138*, e23106.

[36] Fiorio, J. L.; Garcia, M. A. S.; Gothe, M. L.; Galvan, D.; Troise, P. C.; Conte-Junior, C. A.; Vidinha, P.; Camargo, P. H. C.; Rossi, L. M. Recent Advances in the Use of Nitrogen-Doped Carbon Materials for the Design of Noble Metal Catalysts, *Coord. Chem. Rev.* **2023**, *481*, 215053.

[37] Mollabagher, H.; Taheri, S.; Mojtahedi, M. M.; Seyedmousavi, S. Cu-metal organic frameworks (Cu-MOF) as an environment friendly and economical catalyst for one pot synthesis of tacrine derivatives, *RSC Adv.* **2020**, *10*, 1995–2003.

[38] Shi, C. S.; Xu, R. M.; He, L.; Li, T. H.; Liu, S. J.; Yun, R. R. Endowing nanoparticles with high stability on the hydrogenation reaction by the amino group assisted strategy, *Inorg. Chem.* **2023**, *62*, 13400-13404.

[39] Jiang, Y. S.; Zhang, Z.; Cao, W. L.; Zheng, B. S.; Wang, Z. X.; Yun, R. R. Iron based active sites encapsulated in carbon nanotubes for an efficient hydride process, *ACS Appl. Nano Mater.* **2023**, *6*, 3218-3225.

[40] Shaldehi, T. J.; Zhao, L.; Andreu, T.; Rowshanzamir, S.; Sirés, I. Integration of a Non-Precious Pyrolyzed Cu-Doped ZIF as an Oxygen Depolarized Cathode in an Advanced Chlor-Alkali Electrolyzer, *Electrochim. Acta* **2025**, *522*, 145929.

[41] Liu, C. G.; Wang, M. Y.; Liu, S. H.; Wang, Y. J.; Peng, Y.; Lan, Y.; Liu, Q. Manganese catalyzed asymmetric hydrogenation of quinolines enabled by π–π interaction, *Angew. Chem. Int. Ed.* **2021**, *60*, 5108-5113.

[42] Qian, J. M.; Liu, X.; Zhong, C. L.; Xu, G. F.; Li, H. J.; Zhou, W. H.; You, B.; Wang, F.; Gao, D. Q.; Chao, D. L. Enhanced stability and narrowed D band gap of Ce-doped Co_3O_4 for rechargeable aqueous Zn-air battery, *Adv. Funct. Mater.* **2022**, *33*, 2212021.

[43] Li, M. Y.; Liu, C. B.; Huang, Y.; Han, S. Y.; Zhang, B. Water involving transfer hydrogenation and dehydrogenation of N heterocycles over a bifunctional MoNi4 electrode, *Chin. J. Catal.* **2021**, *42*, 1983-1991.

[44] Li, X.; Tian, J. J.; Liu, N.; Tu, X. S.; Zeng, N. N.; Wang, X. C. Spiro bicyclic bisborane catalysts for metal free chemoselective and enantioselective hydrogenation of quinolines, *Angew. Chem. Int. Ed.* **2019**, *58*, 4664-4668.

[45] Li, S. W.; Cao, R. C.; Xu, M. Q.; Deng, Y. C.; Lin, L. L.; Yao, S. Y.; Liang,

X.; Peng, M.; Gao, Z. R.; Ge, Y. Z.; Liu, J. X.; Li, W. X.; Zhou, W.; Ma, D. Atomically dispersed Ir/α-MoC catalyst with high metal loading and thermal stability for water promoted hydrogenation reaction, *Natl. Sci. Rev.* **2022**, *9*, nwab026.

[46] Hervochon, J.; Dorcet, V.; Junge, K.; Beller, M.; Fischmeister, C. Convenient synthesis of cobalt nanoparticles for the hydrogenation of quinolines in water, *Catal. Sci. Technol.* **2020**, *10*, 4820-4826.

[47] Gong, W. B.; Yuan, Q. L.; Chen, C.; Lv, Y.; Lin, Y.; Liang, C. H.; Wang, G. Z.; Zhang, H. M.; Zhao, H. J. Liberating N CNTs confined highly dispersed Co Nx sites for selective hydrogenation of quinolines, *Adv. Mater.* **2019**, *31*, 1906051-1906057.

[48] Wang, C.; Li, C. Q.; Wu, X. F.; Pettman, A.; Xiao, J. L. pH regulated asymmetric transfer hydrogenation of quinolines in water, *Angew. Chem. Int. Ed.* **2009**, *48*, 6524-6528.

[49] Murugesan, K.; Chandrashekhar, V. G.; Kreyenschulte, C.; Beller, M.; Jagadeesh, R. V. A general catalyst based on cobalt core shell nanoparticles for the hydrogenation of N heteroarenes including pyridines, *Angew. Chem. Int. Ed.* **2020**, *59*, 17408-17412.

[50] Hamza, A.; Moock, D.; Schlepphorst, C.; Schneidewind, J.; Baumann, W.; Glorius, F. Unveiling a key catalytic pocket for the ruthenium NHC catalysed asymmetric heteroarene hydrogenation, *Chem. Sci.* **2022**, *13*, 985-995.

[51] Dobereiner, G. E.; Nova, A.; Schley, N. D.; Hazari, N.; Miller, S. J.; Eisenstein, O.; Crabtree, R. H. Iridium catalyzed hydrogenation of N heterocyclic compounds under mild conditions by an outer sphere pathway, *J. Am. Chem. Soc.* **2011**, *133* ,7547-7562.

Electronic Supplementary Material

Cu nanoparticles coated with porous N-doped carbon for the selective hydrogenation of quinolines under mild conditions

Guanyu Wang [1§], Zan Zhang[1§], Taofen Wang[2], Zuxian Cai[1], Baishu Zheng[1](✉), Zhaoxu Wang[1], Ruirui Yun[3] (✉), Zilong Tang[1] (✉), and Hu Zhou[1](✉)

[1] *Key Laboratory of Theoretical Organic Chemistry and Function Molecule of Ministry of Education, Hunan Provincial Key Laboratory of Controllable Preparation and Functional Application of Fine Polymers, Hunan Provincial Key Laboratory of Advanced Materials for New Energy Storage and Conversion, School of Chemistry and Chemical Engineering, Hunan University of Science and Technology, Xiangtan 411201, China*

[2] School of Physics and Electronics, *Hunan University of Science and Technology, Xiangtan 411201, China*

[3] *The Key Laboratory of Functional Molecular Solids Ministry of Education, College of Chemistry and Materials Science, Anhui Normal University, Wuhu 214001, China*

[§] *Guanyu Wang and Zan Zhang contributed equally to this work.*

Supporting information to https://doi.org/10.26599/NR.2026.94908782

1 Experimental Details

Synthesis of catalysts Cu@NC-T: A mixture of pyridine-2,6-dicarboxylic acid (0.668 g, 4.0 mmol) and $Cu(NO_3)_2{\cdot}3H_2O$ (1.50 g, 6.23 mmol) is dissolved in 21 mL DMF/ methanol/H_2O (1:1:1 in volume). The mixture is sonicated for a few minutes in air and the clear solution is transferred into an autoclave and heated to 85 ℃ for 12 hours and then cooled to the room temperature. The obtained precipitates are centrifuged, washed with DMF and methanol, and dried in the vacuum at 60 ℃ overnight. The above-obtained powder is then pyrolyzed at 700 ℃, 800 ℃, 900 ℃ for 2 hours under an Ar atmosphere with a ramp rate of 5℃ min^{-1}, followed by naturally cooling to room temperature to give the catalysts denoted as Cu@NC-700, Cu@NC-800 and Cu@NC-900, respectively.

Catalytic hydrogenation performance evaluation: Typically, quinoline (0.129 g, 0.1 mmol), ammonborane (1 mmol), catalyst (10.0 mg), and 6.0 mL methanol/H_2O (1:2 in volume) as the solvent are added into in a 25 mL bottle, and the mixed suspension is vigorously stirred at 40 ℃ under 1 atm for 1.5~2 h, the conversion and selectivity of the reactions are detected by gas chromatography-mass spectrometry (GC-MS) using n-hexadecane as internal standard. The catalyst is easily separated from the reaction mixture using an external magnet. The hydrogenation reduction of other quinoline derivatives in this work are carried out by a similar experimental procedure.

Chemicals and apparatus: Unless specifically mentioned, all chemicals were commercially available and used as received without further purification. Powder X-ray diffraction (PXRD) data were collected on a Bruker D8 Advance with Cu K_α radiation (λ = 1.5418 Å) at room temperature. Scanning Electron Microscopy (SEM) was conducted on Hitachi 8100. Raman experiments were conducted on a LABRAMHR spectrometer (France) using the green line of an argon laser (λ = 514.5 nm) as the excitation source. X-ray photoelectron spectroscopy (XPS) analysis were conducted on ESCALAB 250 Xi X-ray photoelectron spectrometer using Al K_α radiation. The Nitrogen adsorption isotherms of the samples at 77 K were carried out by the Micromertics ASAP 2020 M+C.

2 Computational details

All of the density functional theory (DFT) calculations were performed using the Perdew–Burke–Ernzerhof (PBE) functional [1], with the long-range dispersion correction included within the Grimme's scheme (DFT-D3) [2], as implemented in VASP codes[3-6]. The kinetic energy cutoff was 400 eV. In all of the cases, the vacuum was set to 50 Å. A Monkhorst–Pack grid of size of 3 × 3 × 1 was used to sample the surface Brillouin zone, which was found to give reliable results based on our testing calculations. The convergence criteria of the energy and force were set to 10^{-5} eV and 0.03 eV/Å, respectively. The vacuum space of 15 Å was set to avoid the periodic interaction. A p (2×2) supercell with a three-layer Cu (111) slab was used as the substrate and a one-layer consisting of C and N atoms as the shell on Cu (111). In this case, the top four layers, including the absorbed species, were allowed to fully relax, whereas the rest was frozen in the bulk positions.

The geometry optimization was performed until the forces on each ion were reduced below 0.02 eV/Å.

The adsorption energy (E_{ads}) was computed as

$$E_{ads} = E_{adsorbate/adsorbent} - E_{adsorbate} - E_{adsorbent} \quad (1)$$

where the $E_{adsorbate/adsorbent}$, $E_{adsorbate}$, and $E_{adsorbent}$ energies are for tThe total energy of the adsorbent adsorbed on the catalyst surface, the energy of the adsorbent alone, and the energy of the surface alone, respectively. For the reaction profiles, the energy for each state was corrected by adding the Gibbs energy computed at T = 313 K by

Address correspondence to Baishu Zheng, zbaishu@163.com; Ruirui Yun, ruirui58@ahnu.edu.cn; Zilong Tang, zltang@hnu.edu.cn; Hu Zhou, zhouhu2006@163.com

$$\Delta G = \Delta E_{ZPE} + \Delta E - T\Delta S \quad (2)$$

where theΔE_{ZPE}, ΔE, and TΔS represent the change in the zero-point energy, the energy difference directly obtained by DFT calculations, and the entropy correction, respectively[7].

3 Supplementary Figures

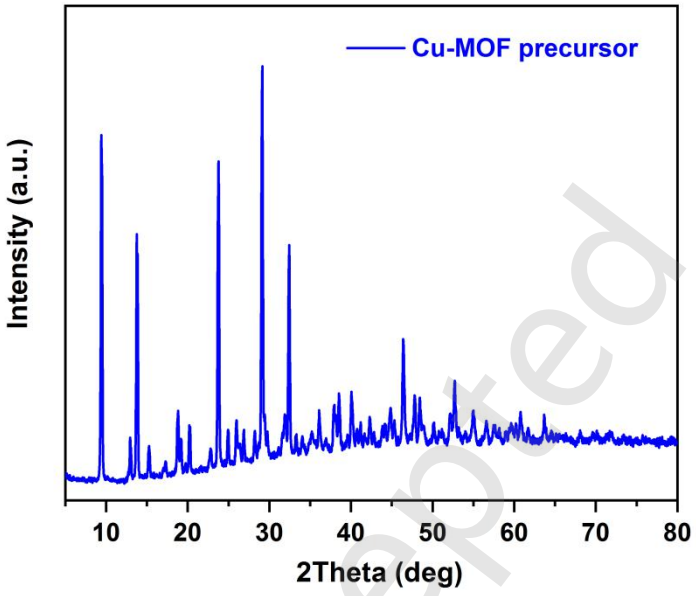

Figure S1 The PXRD patterns of Cu-MOF precursor.

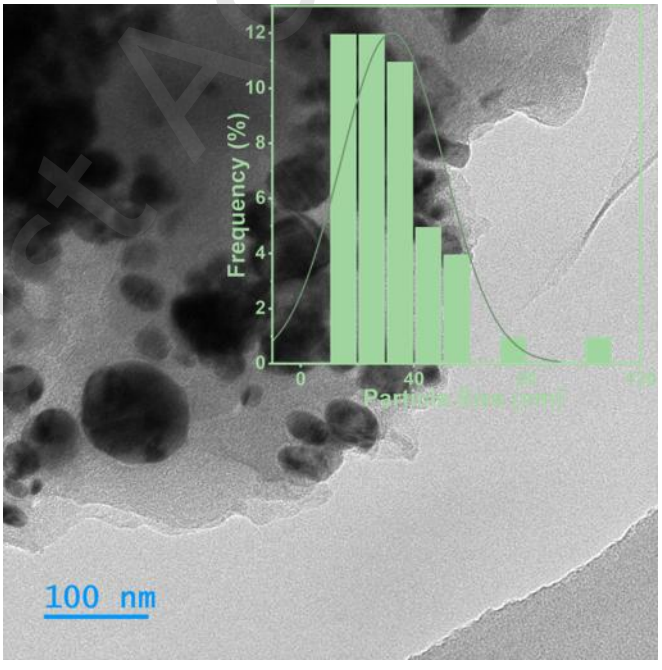

Figure S2 TEM images and Cu particle size distribution of Cu@NC-700.

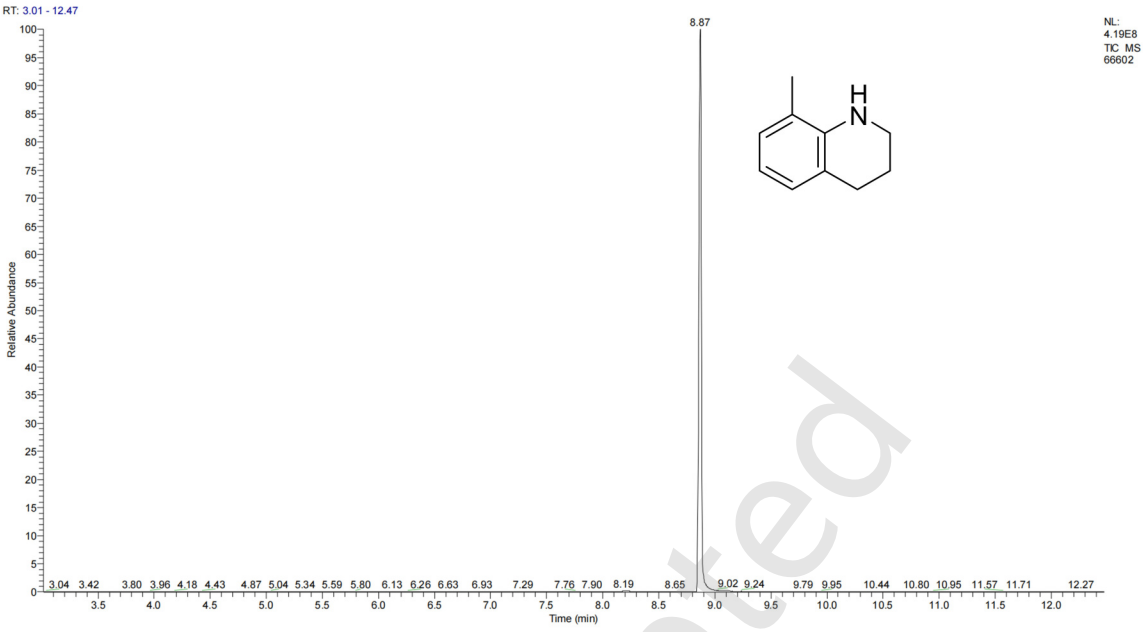

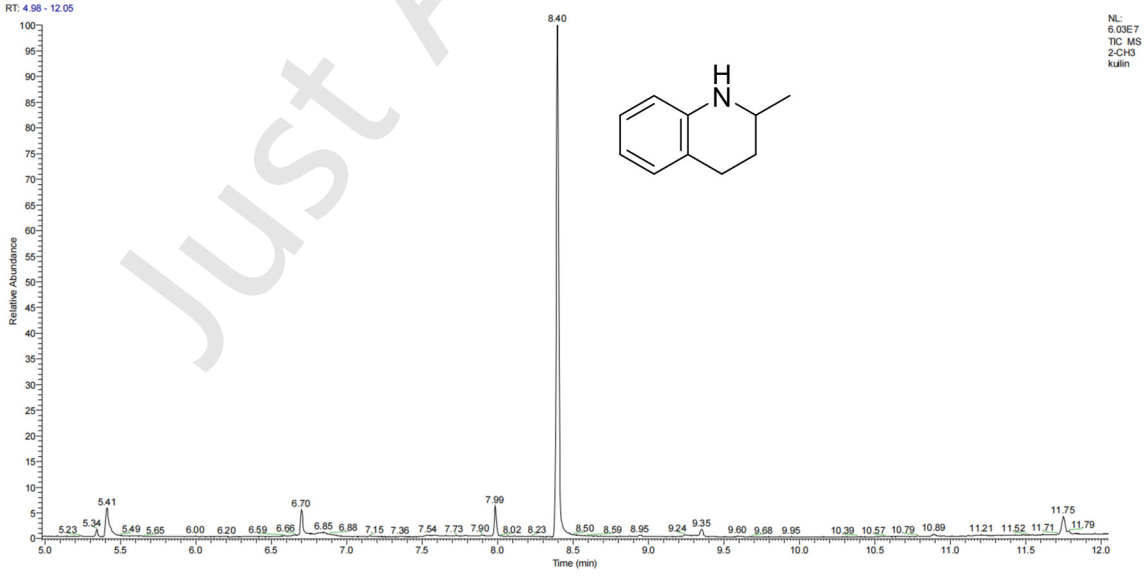

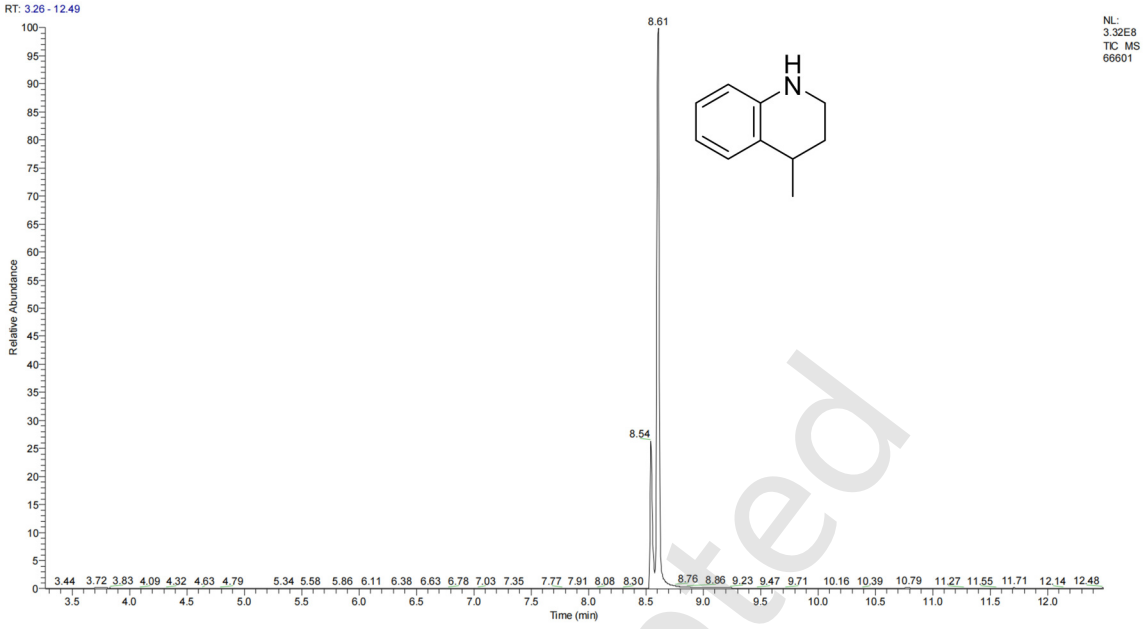

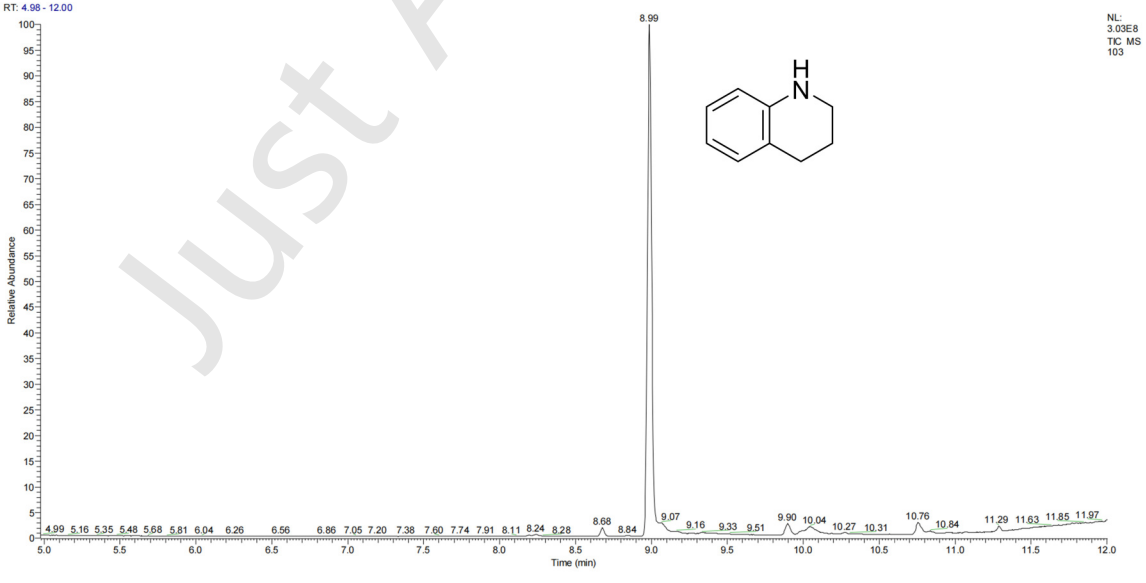

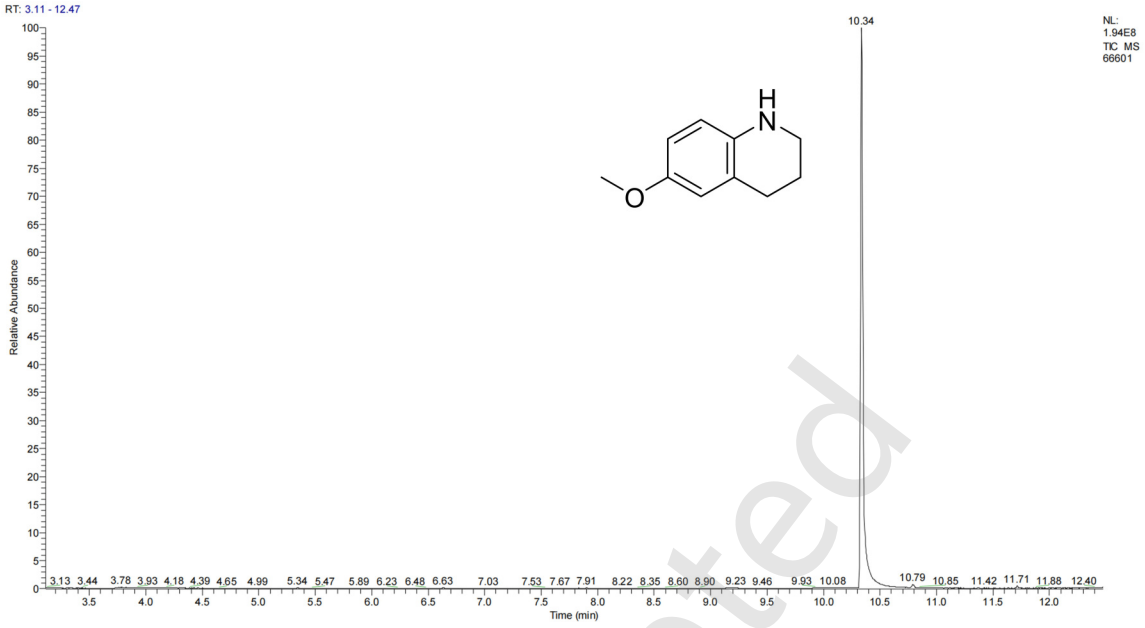

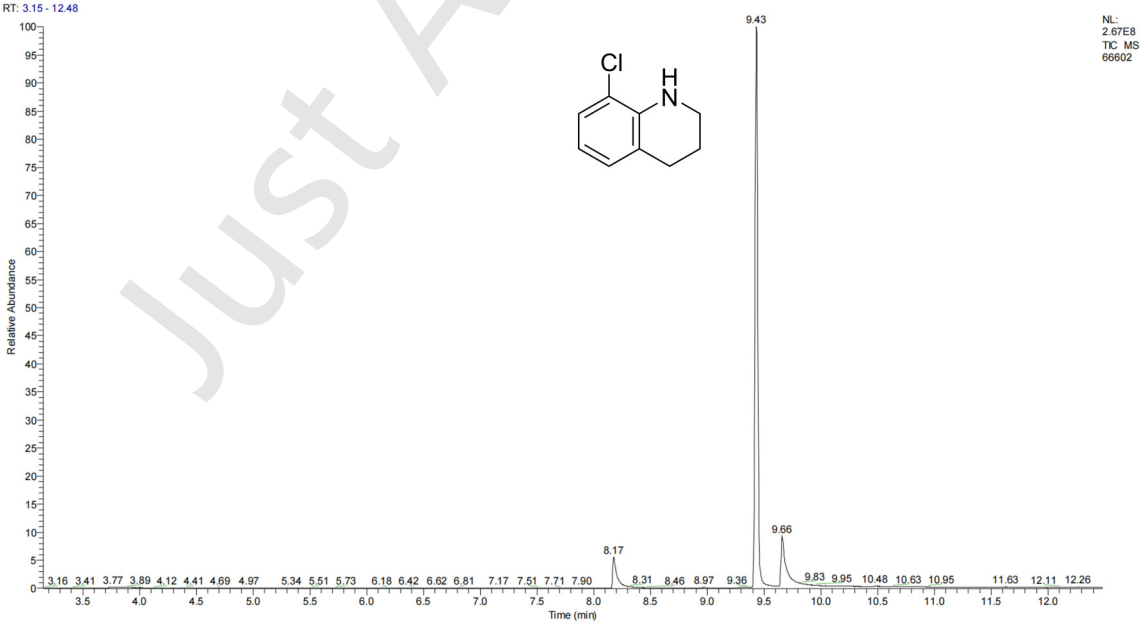

Figure S3 Characterization of compounds 1-8 (Table 1) by gas chromatography-mass spectrometry (GC-MS).

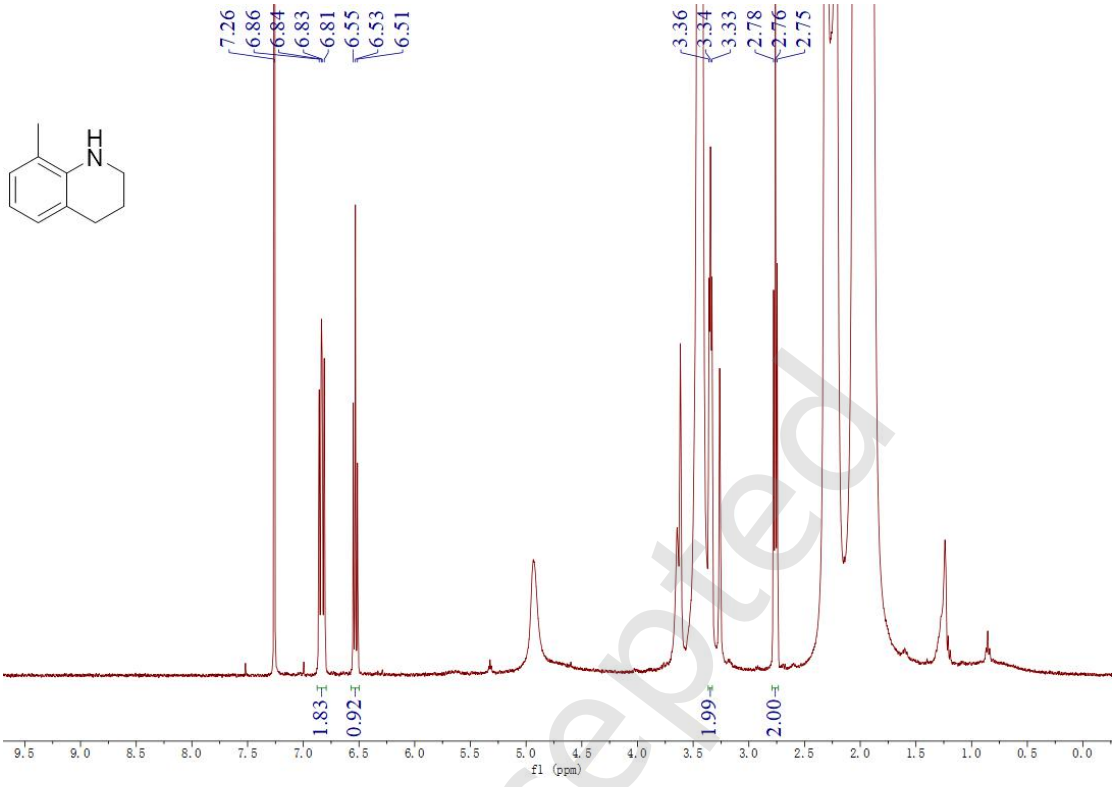

^{1}H NMR of 8-methyl-1,2,3,4-tetrahydroquinoline reaction mixed solution (400 MHz, $CDCl_3$).

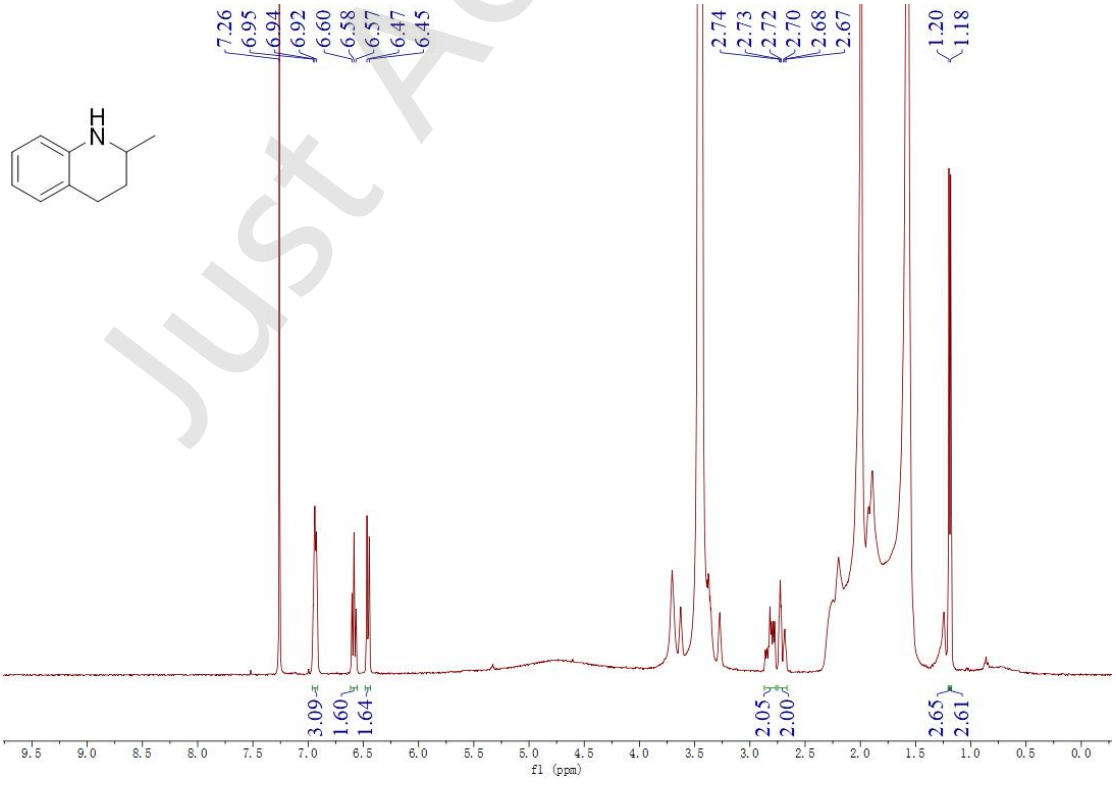

^{1}H NMR of 2-methyl-1,2,3,4-tetrahydroquinoline reaction mixed solution (400 MHz, $CDCl_3$).

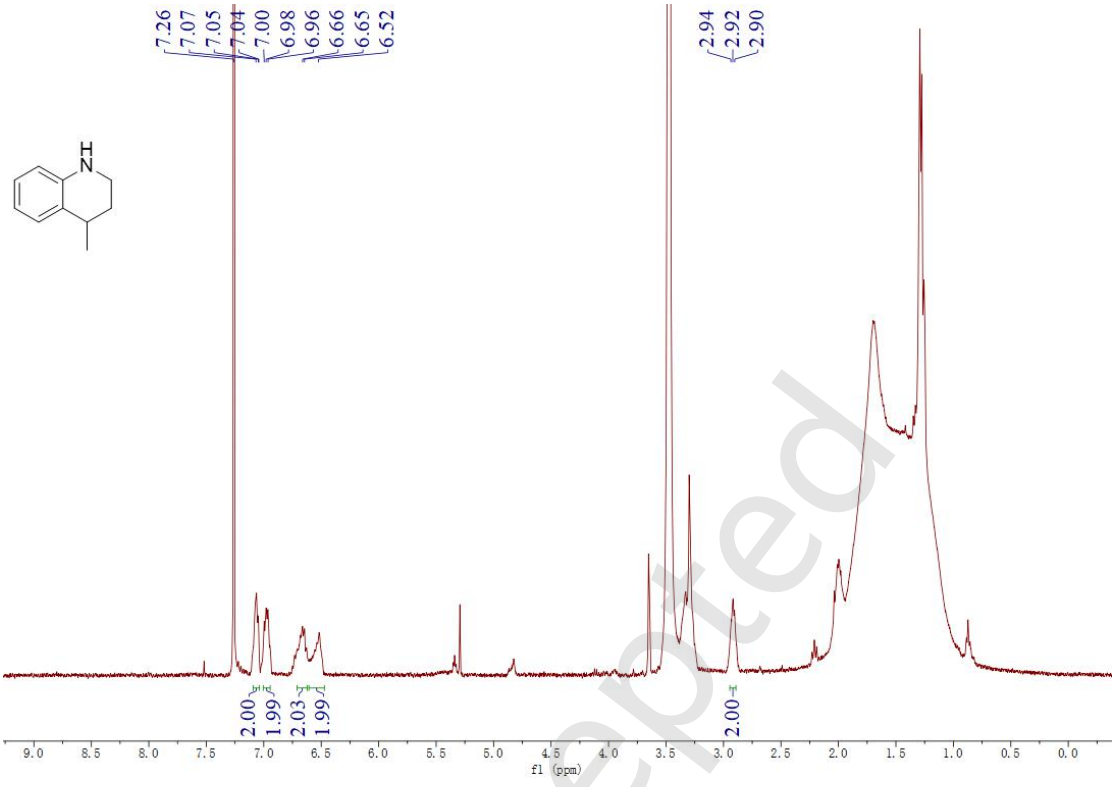

^{1}H NMR of 4-methyl-1,2,3,4-tetrahydroquinoline reaction mixed solution (400 MHz, $CDCl_3$).

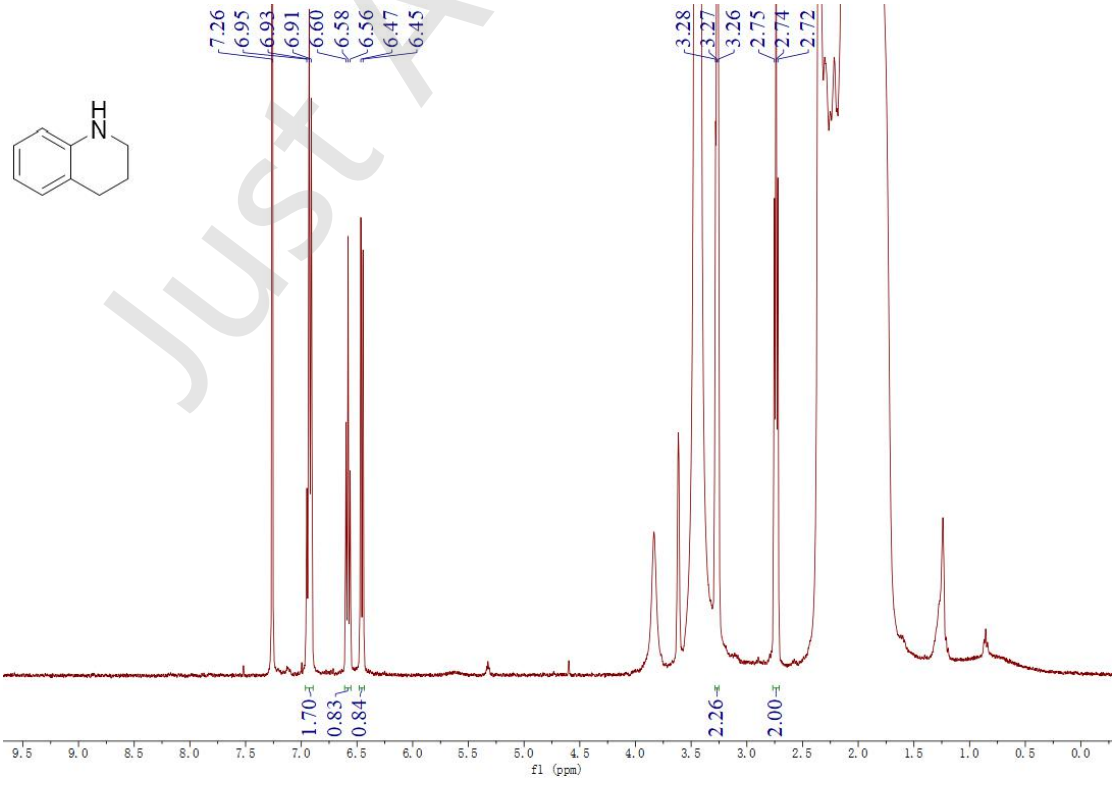

^{1}H NMR of 1,2,3,4-tetrahydroquinoline reaction mixed solution (400 MHz, $CDCl_3$).

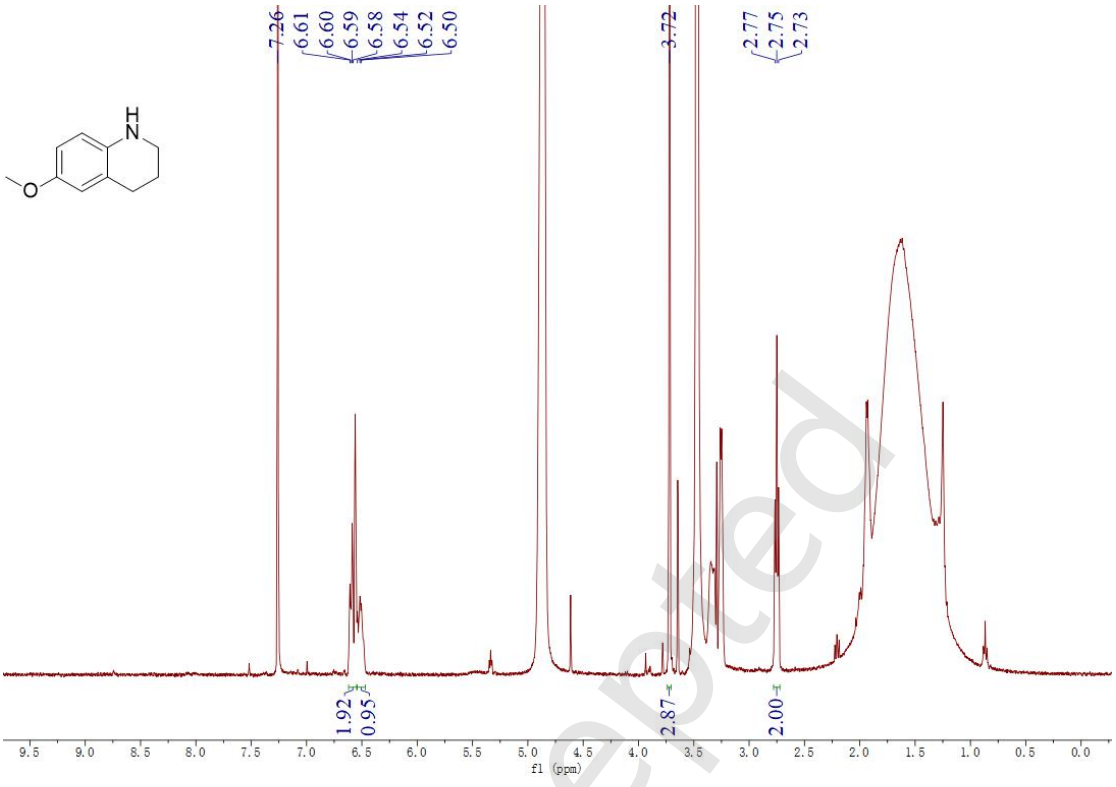

^{1}H NMR of 6-methoxy-1,2,3,4-tetrahydroquinoline reaction mixed solution (400 MHz, $CDCl_3$).

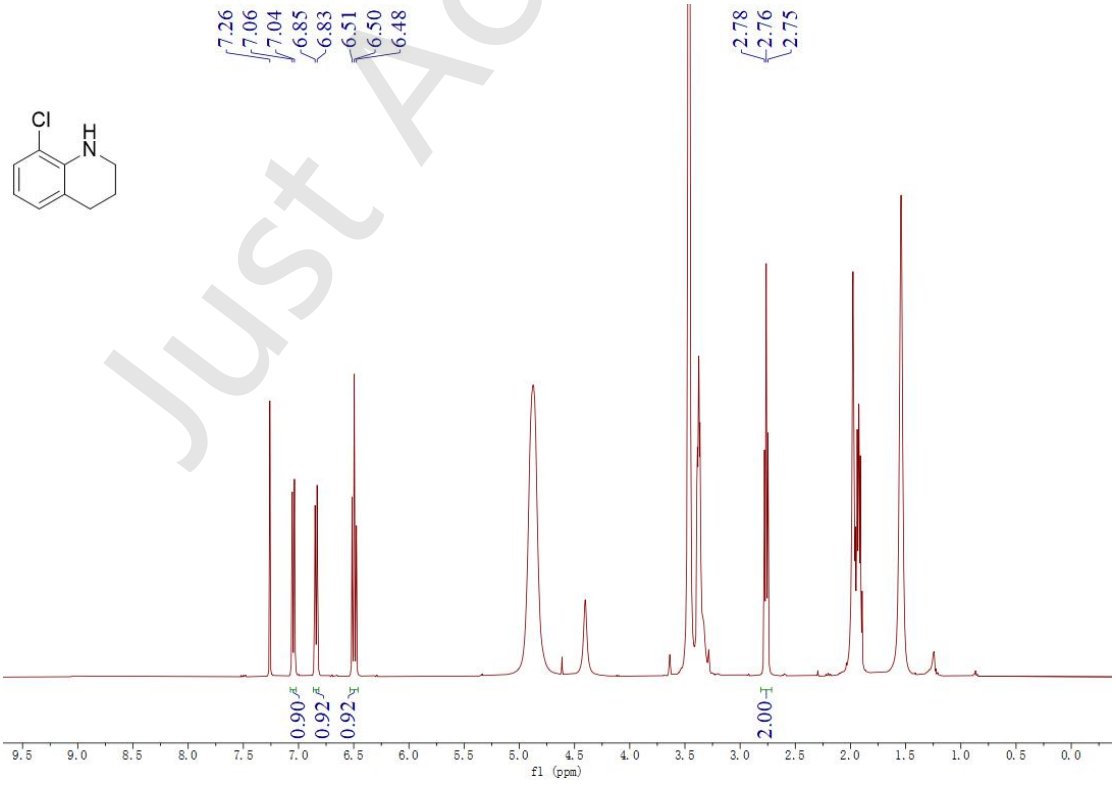

^{1}H NMR of 8-chloro-1,2,3,4-tetrahydroquinoline reaction mixed solution (400 MHz, $CDCl_3$).

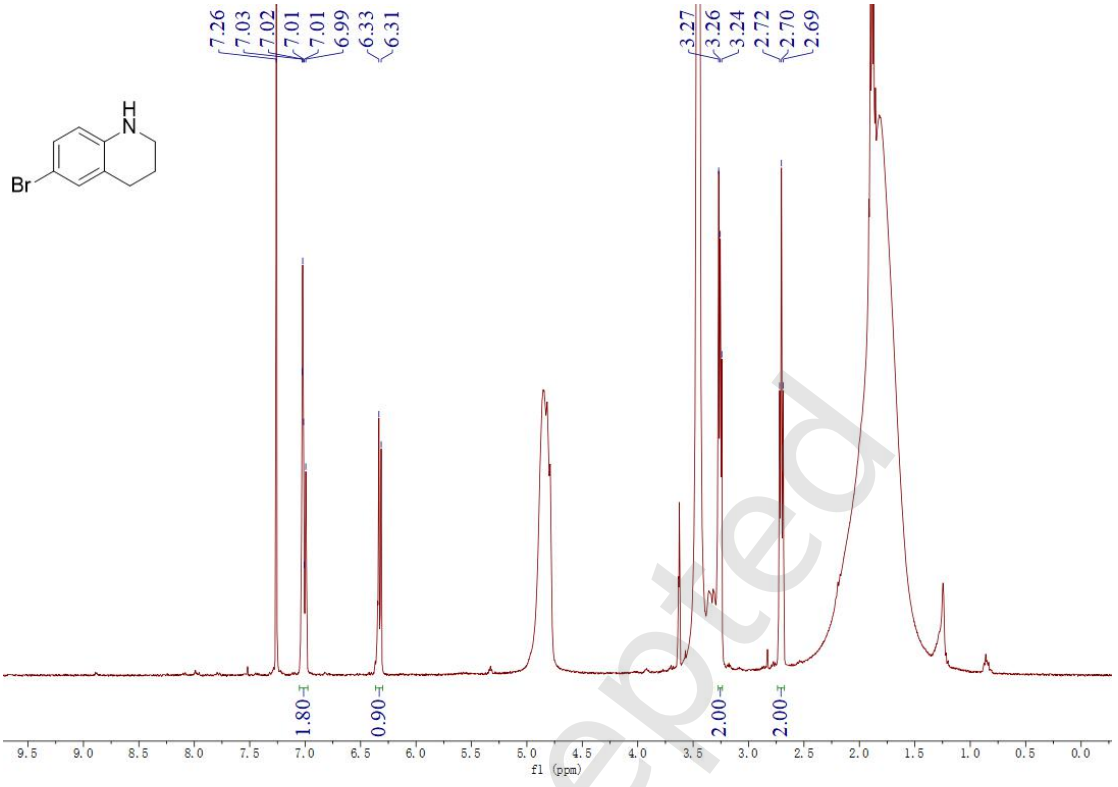

^{1}H NMR of 6-bromo-1,2,3,4-tetrahydroquinoline reaction mixed solution (400 MHz, $CDCl_3$).

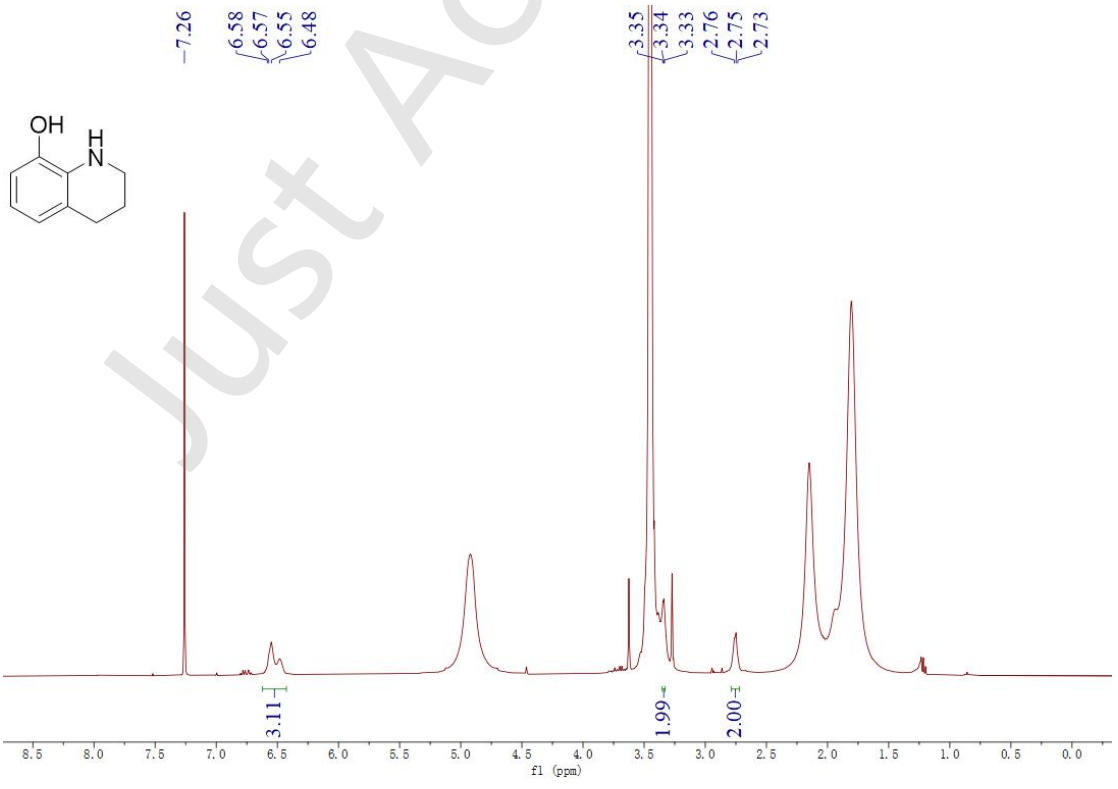

^{1}H NMR of 1,2,3,4-tetrahydroquinolin-8-ol reaction mixed solution (400 MHz, $CDCl_3$).

Figure S4 ^{1}H NMR spectra of the crude reaction mixtures corresponding to compounds 1-8 in Table 1.

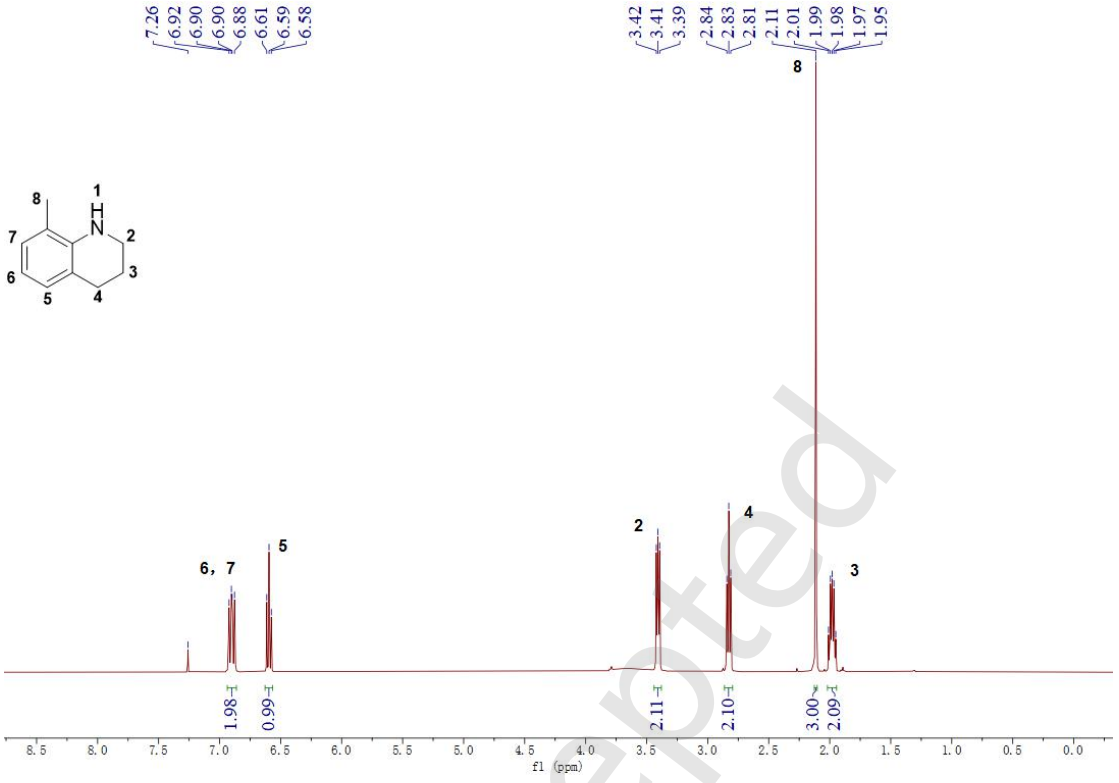

^{1}H NMR of 8-methyl-1,2,3,4-tetrahydroquinoline (400 MHz, $CDCl_3$). ^{1}H NMR (400 MHz, $CDCl_3$) δ 6.90 (dd, J = 10.1, 7.8 Hz, 2H), 6.59 (t, J = 7.4 Hz, 1H), 3.44 – 3.38 (m, 2H), 2.83 (t, J = 6.4 Hz, 2H), 2.11 (s, 3H), 1.98 (p, J = 11.8, 6.3 Hz, 2H).

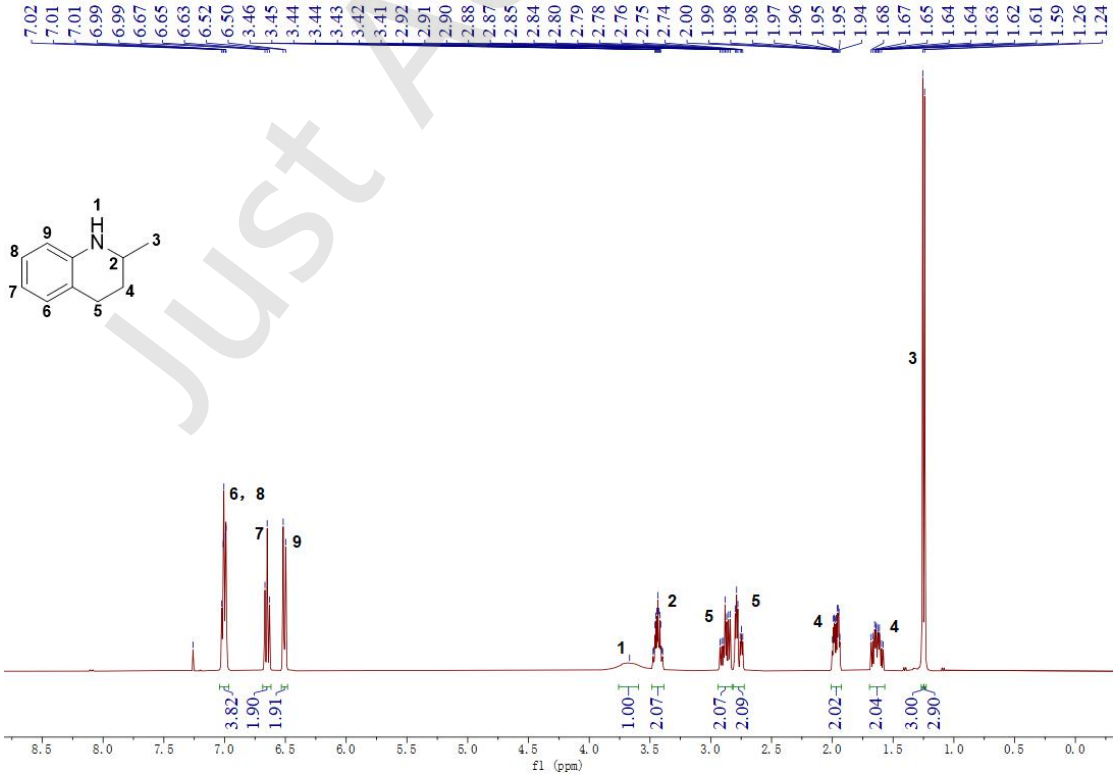

^{1}H NMR of 2-methyl-1,2,3,4-tetrahydroquinoline (400 MHz, $CDCl_3$). ^{1}H NMR (400 MHz, $CDCl_3$) δ 7.04 – 6.97 (m, 4H), 6.65 (t, J = 7.3 Hz, 2H), 6.51 (d, J = 8.2 Hz, 2H), 3.67 (s, 1H), 3.48 – 3.39 (m, 2H), 2.94 – 2.83 (m, 2H), 2.82 – 2.72 (m, 2H), 2.01 – 1.93 (m, 2H), 1.69 – 1.57 (m, 2H), 1.26 (s, 3H), 1.24 (s, 3H).

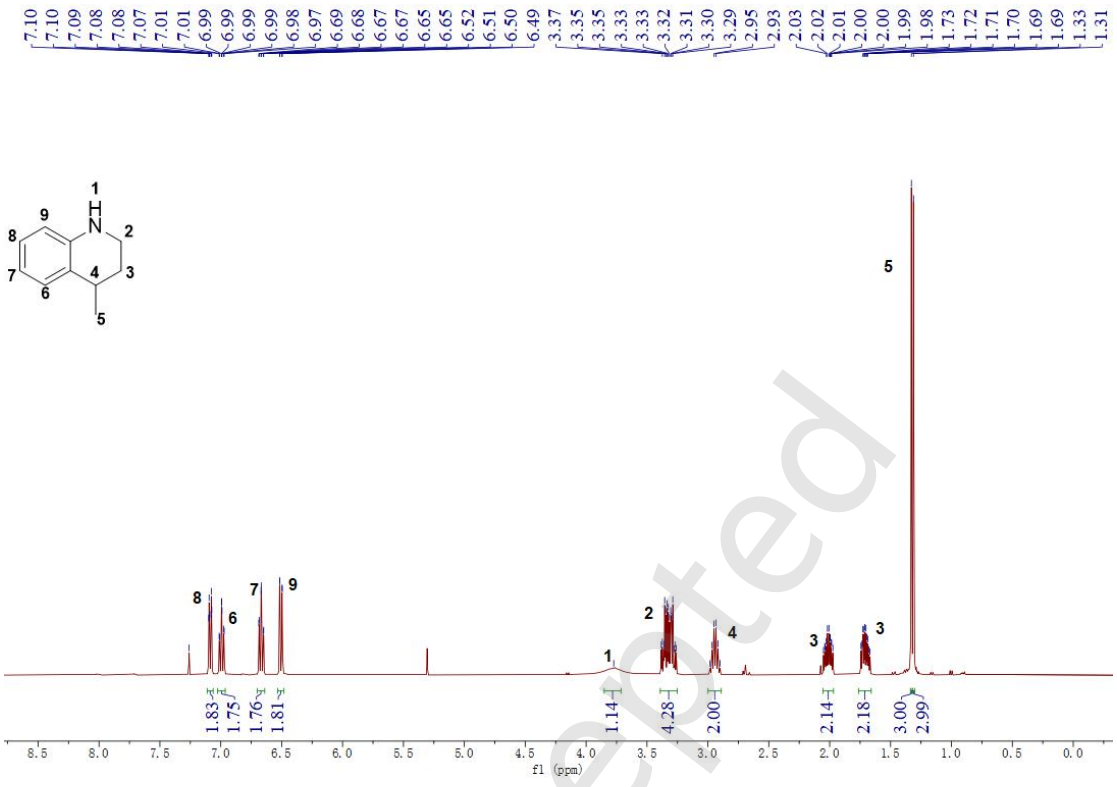

^{1}H NMR of 4-methyl-1,2,3,4-tetrahydroquinoline (400 MHz, $CDCl_3$). ^{1}H NMR (400 MHz, $CDCl_3$) δ 7.09 (dt, J = 7.5, 1.2 Hz, 2H), 7.04 – 6.95 (m, 2H), 6.67 (td, J = 7.4, 1.2 Hz, 2H), 6.51 (dd, J = 8.0, 0.9 Hz, 2H), 3.77 (s, 1H), 3.41 – 3.24 (m, 4H), 3.00 – 2.88 (m, 2H), 2.07 – 1.95 (m, 2H), 1.77 – 1.65 (m, 2H), 1.33 (s, 3H), 1.31 (s, 3H).

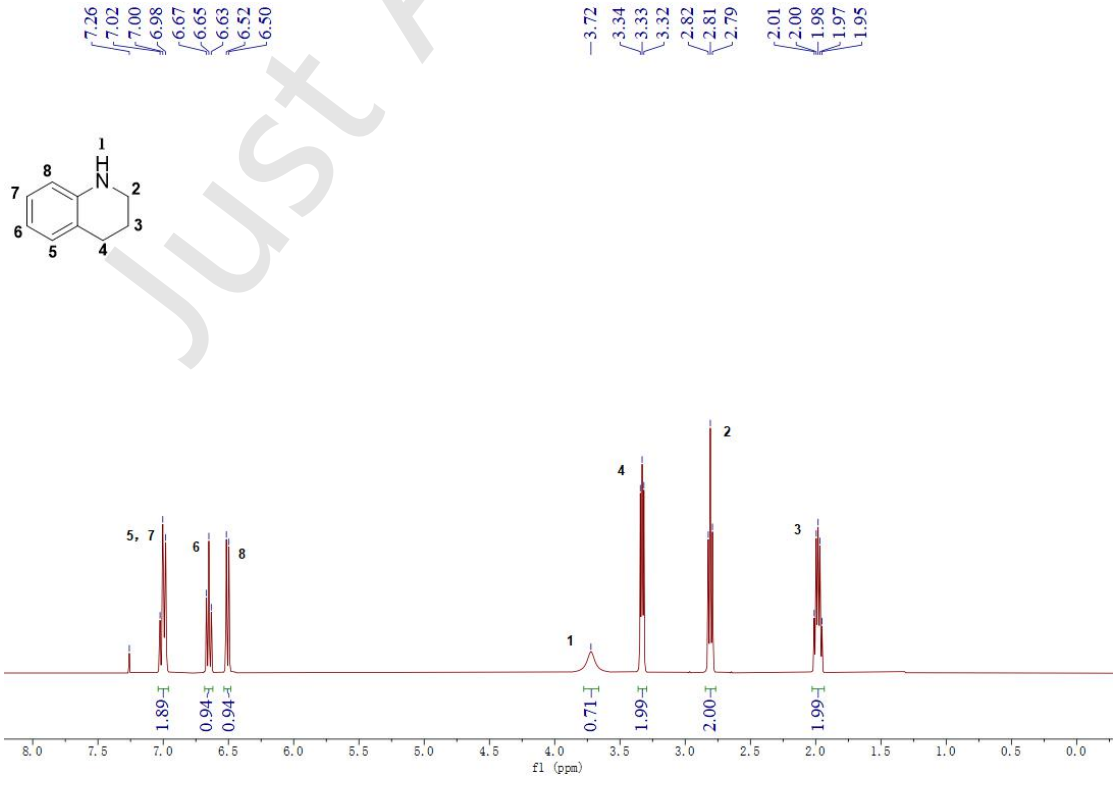

^{1}H NMR of 1,2,3,4-tetrahydroquinoline (400 MHz, $CDCl_3$). ^{1}H NMR (400 MHz, $CDCl_3$) δ 7.04 – 6.96 (m, 2H), 6.65 (t, J = 7.4 Hz, 1H), 6.51 (d, J = 7.9 Hz, 1H),

3.72 (s, 1H), 3.36 – 3.30 (m, 2H), 2.81 (t, J = 6.4 Hz, 2H), 1.98 (p, J = 11.9, 6.3 Hz, 2H).

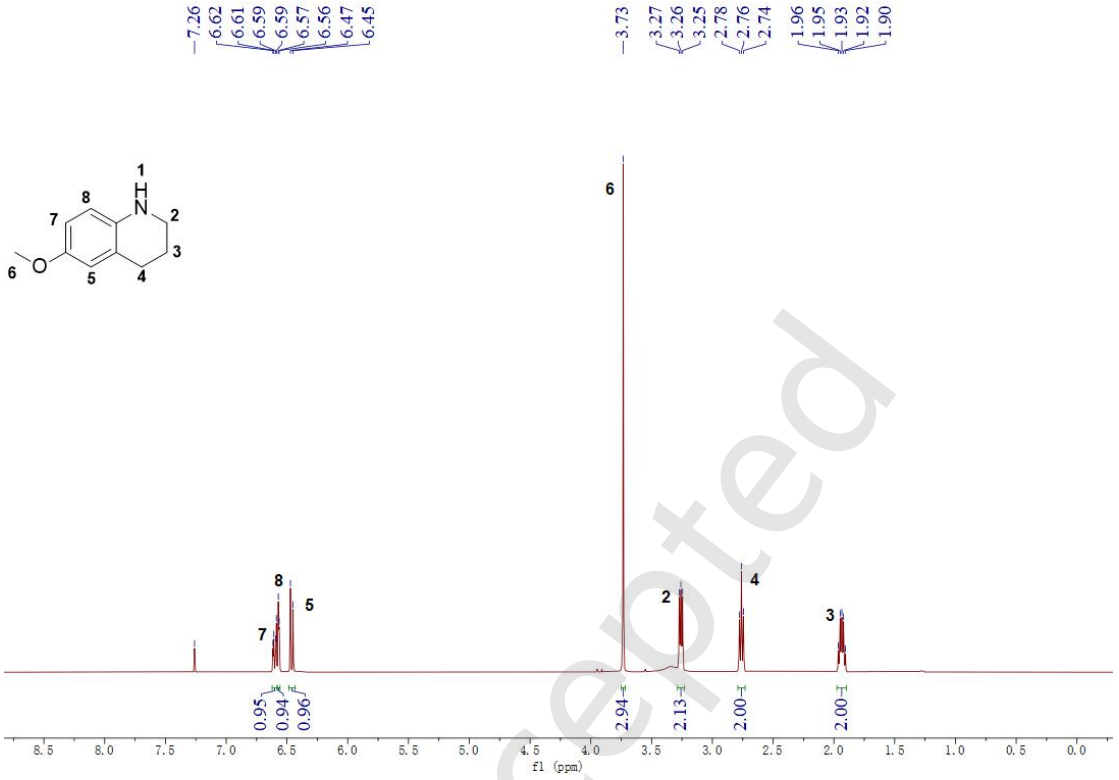

^{1}H NMR of 6-methoxy-1,2,3,4-tetrahydroquinoline (400 MHz, $CDCl_3$). ^{1}H NMR (400 MHz, $CDCl_3$) δ 6.60 (dd, J = 8.5, 2.8 Hz, 1H), 6.57 (d, J = 2.7 Hz, 1H), 6.46 (d, J = 8.5 Hz, 1H), 3.73 (s, 3H), 3.29 – 3.23 (m, 2H), 2.76 (t, J = 6.5 Hz, 2H), 1.93 (p, J = 12.0, 6.4 Hz, 2H).

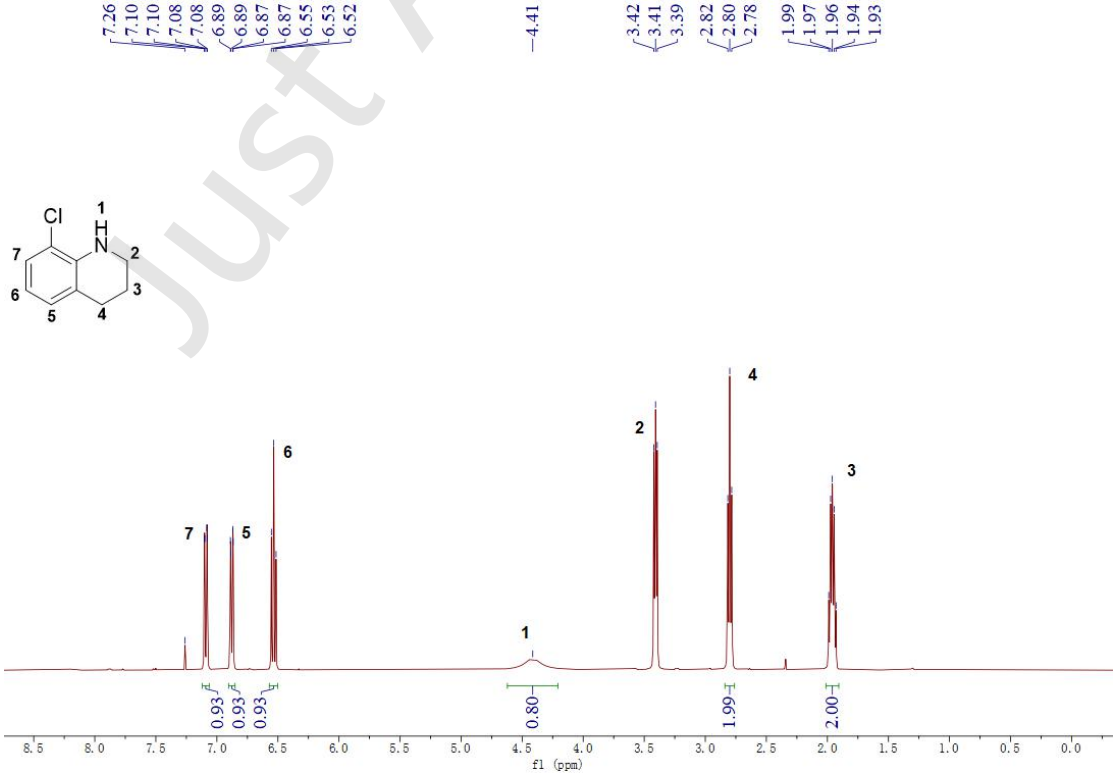

^{1}H NMR of 8-chloro-1,2,3,4-tetrahydroquinoline (400 MHz, $CDCl_3$). ^{1}H NMR (400 MHz, $CDCl_3$) δ 7.09 (dd, J = 8.0, 1.5 Hz, 1H), 6.88 (dd, J = 7.4, 1.5 Hz, 1H),

6.53 (t, J = 7.7 Hz, 1H), 4.41 (s, 1H), 3.44 – 3.37 (m, 2H), 2.80 (t, J = 6.4 Hz, 2H), 1.96 (p, J = 12.3, 6.2 Hz, 2H).

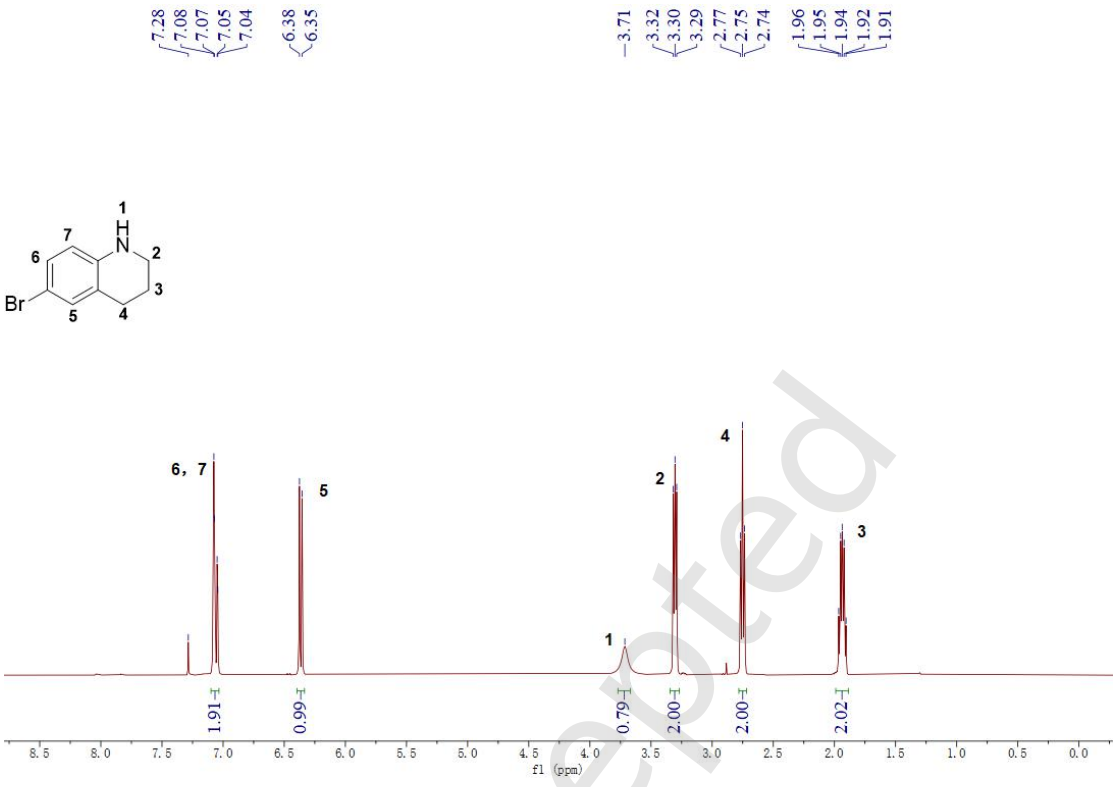

^{1}H NMR of 6-bromo-1,2,3,4-tetrahydroquinoline (400 MHz, $CDCl_3$). ^{1}H NMR (400 MHz, $CDCl_3$) δ 7.06 (dd, J = 10.7, 2.2 Hz, 2H), 6.36 (d, J = 8.3 Hz, 1H), 3.71 (s, 1H), 3.34 – 3.27 (m, 2H), 2.75 (t, J = 6.4 Hz, 2H), 1.99 – 1.89 (m, 2H).

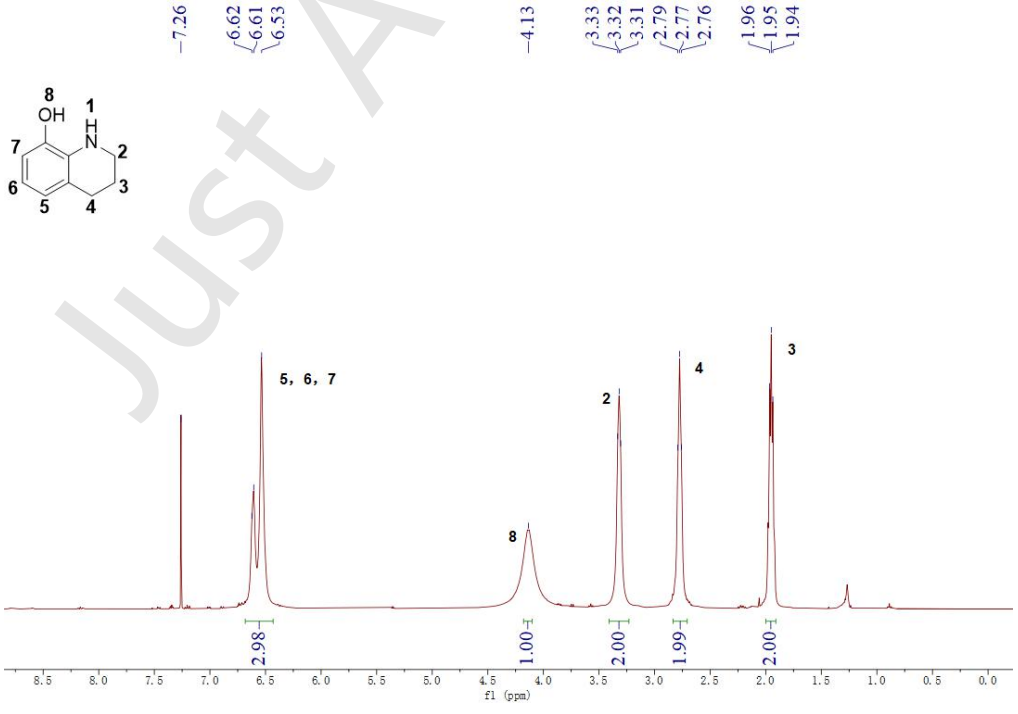

^{1}H NMR of 1,2,3,4-tetrahydroquinolin-8-ol (400 MHz, $CDCl_3$). ^{1}H NMR (400 MHz, $CDCl_3$) δ 6.67 – 6.44 (m, 3H), 4.13 (s, 1H), 3.32 (t, J = 5.4 Hz, 2H), 2.77 (t, J = 6.6 Hz, 2H), 1.95 (p, J = 6.1 Hz, 2H).

Figure S5 Characterization of compounds 1-8 (Table 1) by ^{1}H NMR

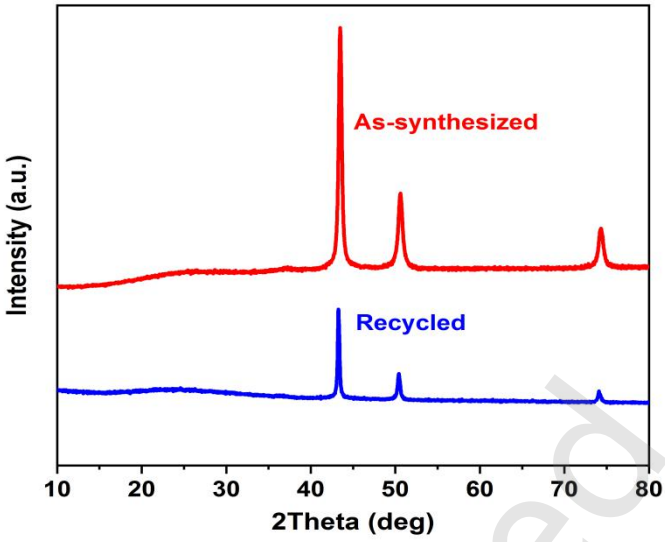

Figure S6 The PXRD patterns of as-synthesized and recycled Cu@NC-900.

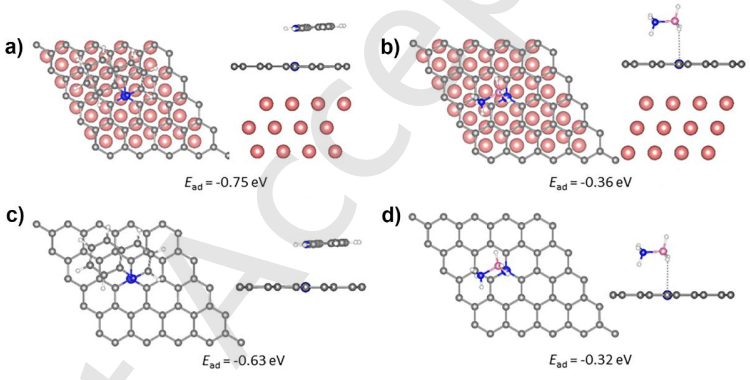

Figure S7 (a-b) Cu@NC structure of adsorbed quinoline and amborane; (c-d) NC adsorption structure of quinoline and aminoborane.

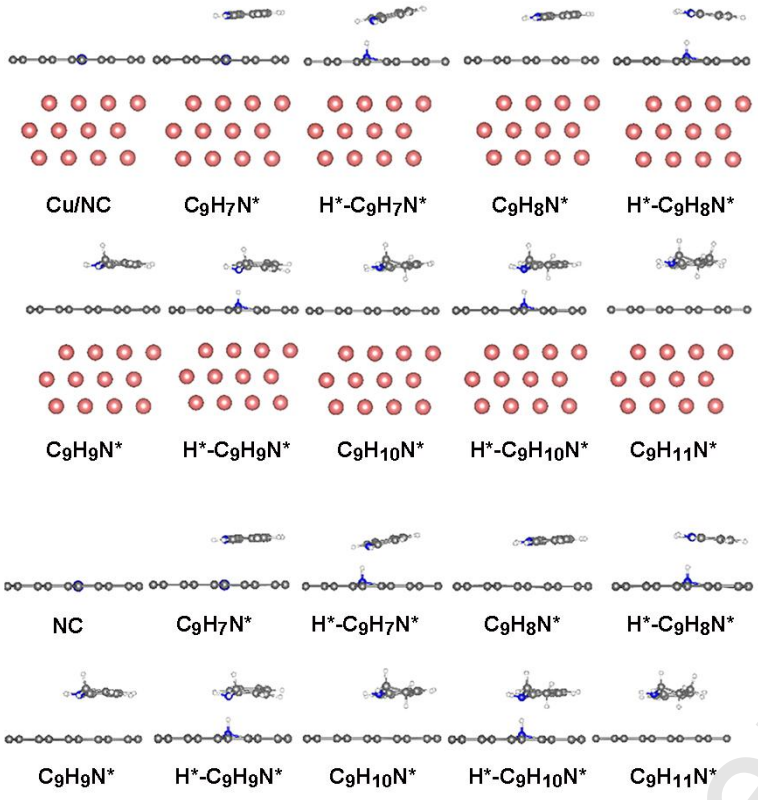

Figure S8 The optimized configuration of catalyst and hydrogenation reaction intermediates.

4 Tables

Table S1. Performance of different catalysts in the hydrogenation of quinoline.

Entry	Catalysts	Temp./℃	Time/h	Conversion/%	Selectivity/%
1	Cu-MOF precursor	40	1	<1	–
2	Cu@NC-700	40	1	6.1	>99
3	Cu@NC-800	40	1	17.19	>99
4	Cu@NC-900	40	1	>99	>99

Table S2. Performance comparison of quinoline hydrogenation of other catalysts reported in the literature.

Entry	Catalysts	Temp./ °C	Time/h	Conv./%	Select./%	Ref
1	Cu/NC-900	40	1	>99	>99	This work
2	Co-F	25	–	94	99	8
3	$MoNi_4$	25	10	33	99	9
4	Spiro-bicyclic bisborane	25	24	97	91	10
5	NNP-pincer manganese	80	16	97	97	11
6	Ir/α-MoC	120	1	95	99	12
7	Co nanoparticles	130	17	100	78	13
8	Co-SA/AC@N-CNTs-L	100	3	97.4	99.1	14
9	$[(Cp^*RhCl_2)_2]$	40	0.5	96	97	15
10	Co-pyromellitic acid@SiO_2	70	24	97	–	16
11	Co-Mo-S	150	10	94	91	17

一、References

[1] Perdew, J. P.;Burke, K.; Ernzerhof, M. Generalized gradient approximation made simple. *Phys. Rev. Lett.* **1996**, *77*, 3865-3868.

[2] Grimme, S. Semiempirical GGA-type density functional constructed with a long-range dispersion correction. *J. Comput. Chem.* **2006**, *27*, 1787-1799.

[3] Kresse, G. AB-INITIO MOLECULAR-DYNAMICS FOR LIQUID-METALS. *J. Non-Cryst. Solids* **1995**, *193*, 222-229.

[4] Kresse, G.; Hafner, J. AB-INITIO MOLECULAR-DYNAMICS SIMULATION OF THE LIQUID-METAL AMORPHOUS-SEMICONDUCTOR TRANSITION IN GERMANIUM. *Phys. Rev. B* **1994**, *49*, 14251-14269.

[5] Kresse, G.; Furthmuller, J. Efficiency of ab-initio total energy calculations for metals and semiconductors using a plane-wave basis set. *Comput. Mater. Sci.* **1996**, *6*, 15-50.

[6] Kresse, G.; Furthmuller, J. Efficient iterative schemes for ab initio total-energy calculations using a plane-wave basis set. *Phys. Rev. B* **1996**, *54*, 11169-11186.

[7] Tian, Z.;Chen, D. L.;He, T.;Yang, P. Y.;Wang, F. F.;Zhong, Y. J.; Zhu, W. D. Theoretical Evidence on the Confinement Effect of Pt@UiO-66-NH2 for

Cinnamaldehyde Hydrogenation. *J. Phys. Chem. C* **2019**, *123*, 22114-22122.

[8] Qian, J.; Liu, X.; Zhong, C.; Xu, G.; Li, H.; Zhou, W.; You, B.; Wang, F.; Gao, D. ; Chao, D. Enhanced stability and narrowed D-band gap of Ce-doped Co_3O_4 for rechargeable aqueous Zn-air battery, *Adv. Funct. Mater.* **2022**, *33*, 2212021-2212029.

[9] Li, M.; Liu, C.; Huang, Y.; Han, S.; Zhang, B. Water involving transfer hydrogenation and dehydrogenation of N heterocycles over a bifunctional $MoNi_4$ electrode, *Chin. J. Catal.* **2021**, *42* ,1983-1991.

[10] Li, X.; Tian, J. J.; Liu, N.; Tu, X. S.; Zeng, N. N.; Wang, X.C. Spiro-bicyclic bisborane catalysts for metal-free chemoselective and enantioselective hydrogenation of quinolines, *Angew. Chem. Int. Ed.* **2019** ,*58* , 4664-4668.

[11] Liu, C.; Wang, M.; Liu, S. ;Wang, Y.; Peng, Y. ;Lan, Y.; Liu, Q. Manganese-catalyzed asymmetric hydrogenation of quinolines enabled by π–π interaction, *Angew. Chem. Int. Ed.* **2021**, *60*, 5108-5113.

[12] Li, S.; Cao, R.; Xu, M.; Deng, Y.; Lin, L.; Yao, S.; Liang, X.; Peng, M.; Gao, Z.; Ge, Y.; Liu, J. X.; Li, W. X.; Zhou, W.; Ma, D. Atomically dispersed Ir/α-MoC catalyst with high metal loading and thermal stability for water promoted hydrogenation reaction, *Natl. Sci. Rev.* **2022**, *9*, nwab026.

[13] Hervochon, J.; Dorcet, V.; Junge, K.; Beller, M.; Fischmeister, C. Convenient synthesis of cobalt nanoparticles for the hydrogenation of quinolines in water, *Catal. Sci. Technol.* **2020**, *10*, 4820-4826.

[14] Gong, W.; Yuan, Q.; Chen, C.; Lv, Y.; Lin, Y.; Liang, C.; Wang, G.; Zhang, H.; Zhao, H. Liberating N CNTs confined highly dispersed Co Nx sites for selective hydrogenation of quinolines, *Adv. Mater.* **2019**, *31*, 1906051-1906057.

[15] Wang, C.; Li, C.; Wu, X.; Pettman, A.; Xiao, J. pH regulated asymmetric transfer hydrogenation of quinolines in water, *Angew. Chem. Int. Ed.* **2009**, *48*, 6524-6528.

[16] Murugesan, K.; Chandrashekhar, V.G.; Kreyenschulte, C.; Beller, M.; Jagadeesh, R. V. A general catalyst based on cobalt core shell nanoparticles for the hydrogenation of N heteroarenes including pyridines, *Angew. Chem. Int. Ed.* **2020**, *59*, 17408-17412.

[17] Srribes, I.; Liu, L. C.; Dménech-Carbó, A.; Corma, A. Nanolayered cobalt–molybdenum sulfides as highly chemo- and regioselective catalysts for the hydrogenation of quinoline derivatives, *ACS Catal.* **2018**, *8*, 4545–4557.